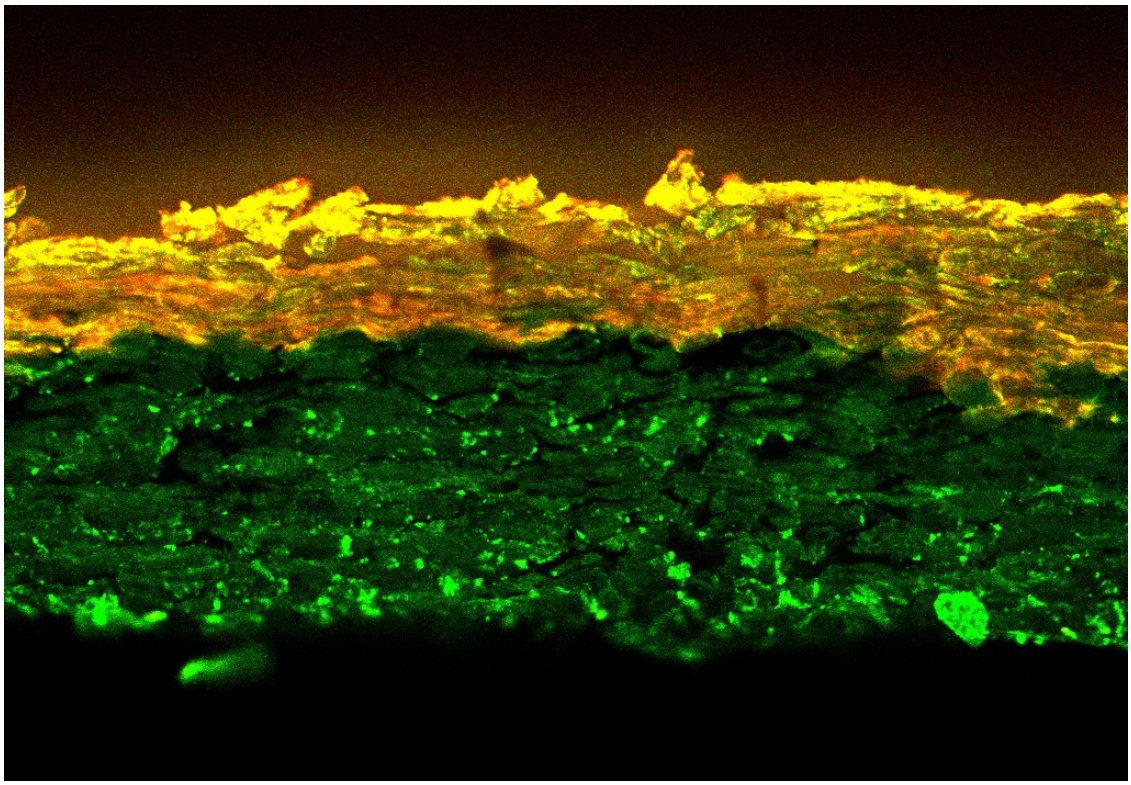

Dynamics of the liquid transport through thin paper

CLSM-observations to investigate the paper straw performance

Master's Thesis in Materials Chemistry

ELLEN EMANUELSSON & EMMA PETTERSSON

DEPARTMENT OF CHEMISTRY AND CHEMICAL ENGINEERING
Chalmers University of Technology
Gothenburg, Sweden 2023
Division of Applied Chemistry
www.chalmers.se

MASTER'S THESIS 2023

Dynamics of the liquid transport through thin paper

CLSM-observations to investigate the paper straw performance

ELLEN EMANUELSSON & EMMA PETTERSSON

CHALMERS
UNIVERSITY OF TECHNOLOGY

Department of Chemistry and Chemical Engineering
Division of Applied Chemistry
CHALMERS UNIVERSITY OF TECHNOLOGY
Gothenburg, Sweden 2023

Dynamics of the liquid transport through thin paper
CLSM-observations to investigate the paper straw performance
ELLEN EMANUELSSON & EMMA PETTERSSON

Supervisors: Niklas Lorén, RISE Agriculture and Food, Chalmers University of Technology, Department of Physics
Camilla Öhgren, RISE Agriculture and Food
Eskil Anderasson, Tetra Pak®
Examiner: Lars Evenäs, Chalmers University of Technology, Chemistry and Chemical Engineering

Master's Thesis 2023
Department of Chemistry and Chemical Engineering
Division of Applied Chemistry
Chalmers University of Technology
SE-412 96 Gothenburg
Sweden
Telephone +46 31 772 1000

Cover: CLSM snapshot of liquid penetration into cross-section thickness of paper straw material.

Typeset in LaTeX
Printed by Chalmers Reproservice
Gothenburg, Sweden 2023

Dynamics of the liquid transport through thin paper
CLSM-observations to investigate the paper straw performance
ELLEN EMANUELSSON & EMMA PETTERSSON
Department of Chemistry and Chemical Engineering
Chalmers University of Technology

Abstract

Single-use plastics, such as drinking straws, are not environmentally friendly and have recently been replaced by paper-based drinking straws to lower the environmental impact. However, straws made from paper do not always meet the consumers expectations since the liquid penetrates into the straw and causes an impair on the mechanical material properties and therefore further development is required. In addition, the paper straw production needs improvement and optimization.

The goals of this project were to characterize different liquids with varying properties, the paper straw material and the interaction between them with the future aim to produce paper-based drinking straws that meet the expectations of the consumers. Liquid characterization was performed by experimental methods such as measuring pH, viscosity and surface tension. To characterize the material, changes in relative humidity were investigated in relation to the cross-section thickness of paper straw material. Contact angle measurements and time-resolved in-situ experiments by confocal laser scanning microscopy, were performed to characterize the paper-liquid interactions, in terms of liquid transport through paper fibers, capillary transport of liquid through pore space and vapor diffusion through pore space.

A set of experiments were performed where the paper material was conditioned to three different climates to investigate the effect and isolate the moisture transport phenomena. The liquid penetration studies were performed with water as a reference. The liquids with increased viscosity, PEG 3000 and PEG 35000 led to the conclusion that the liquid penetration was not affected. Liquids modified with an emulsifier, Tween®20, liquids containing surfactants composed of the commercial brand Yes, and liquids modified to a pH of 2 respectively 9 increased the penetration rate of liquid into the paper straw material compared to water. The penetration rate, however, decreased with the addition of NaCl or saccharose. It was found that the combination of techniques was powerful to investigate the dynamics of the liquid transport through thin paper.

Further, three transport mechanisms did occur during the wetting of the paper strip samples in this work; I) transport through paper fibers, II) capillary transport of liquid through pore space and III) vapor diffusion through pore space. Capillary transport was found to be the dominant mechanism in the case of Yes, while the other modified liquids demonstrated a combination of the three mechanisms.

Keywords: drinking straw, cellulose, penetration rate, transport mechanism, characterize, relative humidity, cross-section thickness, confocal laser scanning microscopy, imbibition, pore space, contact angle, moisture.

Acknowledgements

The master thesis research project was carried out within the Vinnova-project "Real time 4D X-ray microtomography imaging and analysis of water transport mechanisms in sustainable paper straws" (2021-03824), we acknowledge the support.

This project would not have been possible without the supervision and support from our supervisors, Eskil Andreasson, Camilla Öhgren and Niklas Lorén. Thanks for all the discussions and your dedication, but particularly for your optimistic personality, Eskil. It has been a pleasure working with you on the experimental work and discussing results to keep the project moving forward, Camilla. Thank you, Niklas, for your innovative ideas and passion, which guided us in the right direction.

A thank you is also addressed to everyone at the department Agriculture and Food at RISE for their warm welcome and all knowledge they contributed with. Lastly, a thank you is directed to all innovative staff that welcomed us during our visit at Tetra Pak® in Lund. You have impressive expertise and gave us good advice when we had questions and concerns.

Ellen Emanuelsson & Emma Pettersson, Gothenburg, June 2023

List of Acronyms

Below is the list of acronyms that have been used throughout this thesis listed in alphabetical order:

CD	Cross-Direction
CLSM	Confocal Laser Scanning Microscopy
CMC	Critical Micelle Concentration
MD	Machine Direction
M_w	Molecular Weight
PEG	Polyethylene glycol
PS	Print Side
RH	Relative Humidity
RS	Reverse Side

Contents

List of Figures

List of Tables

1
Introduction

In 2021, the world's population was 7.19 billion [3]. There has been an increase in this number annually, and since all humans have a right to access safe food and beverages, modern packaging is important to feed the increasing population in a food-safe way. In a significant way, plastic materials have contributed to this development. Plastic materials have many favorable properties compared to other materials. For example, they are lightweight, have low durability, high versatility and a low price. This makes plastic suitable for a wide range of different applications and the material class has provided many conveniences to humans since its invention [4, 5]. However, plastic waste management systems are lacking in big parts of the world, and since plastics last for hundreds of years in nature, plastic wastes cause environmental pollution and thereby damage to nature. One important action towards the decreased use of plastics was taken in 2021 when the European Commission decided to introduce a restriction regarding single-use plastics [6].

According to the European Commission, single-use plastics are defined as "products that are made wholly or partly of plastic and are typically intended to be used just once or for a short period of time before they are thrown away", for example, plastic drinking straws [6]. This restriction has led to the replacement of traditional plastic drinking straws with straws made of other materials, mainly paper-based materials. Tetra Pak® was the first carton packaging company to launch paper-based straws for beverage cartons in Europe [7]. The restriction of single-use plastics is mainly because of the non-biodegradability and difficulties in the recycling of plastic straws together with poor waste management. When ending up in nature after use, plastic straws can be converted into microplastic residuals by photodegradation and later through food end up in the human body and in animals, endangering health [4].

Even though the paper straws developed so far have a lower environmental impact compared to plastic straws and are cheap to produce, they do not always meet the expectations of the consumers and therefore further development is required. Poor water stability is the main problem with paper straws since absorption of liquids and moisture strongly influences the mechanical properties and hence the drinking experience. After only minutes of use, the paper soaks in the liquid, causing the straw to soften and become difficult to use. Different types of liquids come in contact with paper straws during the production processes and the product's service life, as well as the recycling processes [8]. A better understanding of the interaction between paper-based drinking straws and liquids with different properties is therefore important for further development of the product [9].

Paper-liquid interactions have been quantified previously, however, only according to different extremes of liquid properties [10]. It is therefore in Tetra Pak®'s interest to characterize paper-liquid interactions and dynamics in a more consequent and systematic way using liquids with different properties. To obtain data for future computer modelling that can assist in improving the product's quality and the customer's experience, experiments are necessary for characterizing the paper straw material and the liquids as well as examining the interaction mechanisms between the paper and liquids [11].

1.1 Aim

The objective of this project is to build knowledge and understanding of how the liquid imbibition in paper straw material affects the mechanical material properties in order to develop a deeper understanding of the material structure and behavior.

In order to approach the objective, the thesis has the following goals:

- Characterization of liquids with varying physical properties. The evaluation will be based on surface tension measurements, viscosity measurements and pH measurements.
- Characterization of the paper straw material by evaluation of how relative humidity influences the paper straw material. Information obtained will indicate the influence of the relative humidity in the environment and the temperature gradient in the surroundings.
- Characterization of the interaction between the liquids with varying physical properties and the paper straw material by contact angle measurements and in-situ confocal laser scanning microscopy measurements.
- Quantification and determination of the transport mechanisms occurring when liquids with varying physical properties interact with paper straw material by in-situ confocal laser scanning microscopy measurements combined with image analysis.
- Kinetic evaluation of liquid penetration into paper straw material and swelling behavior of paper straw material by in-situ confocal laser scanning microscopy measurements combined with image analysis.

With the aim of fulfilling the goals, Figure 1.1 shows the thesis deposition in order to achieve them. The in-situ experiments with CLSM are intended to support the understanding of the interaction occurring between paper straw material and the various liquids it is exposed to, during the production processes, the consumer phase and the recycling processes. Owing to the increased understanding, a more accurate characterization could be achieved as well as an increased usage of modeling techniques in the future. This is intended in order to develop an optimal paper straw product that is efficiently produced both from an environmental and economic perspective that meets the consumer's expectations.

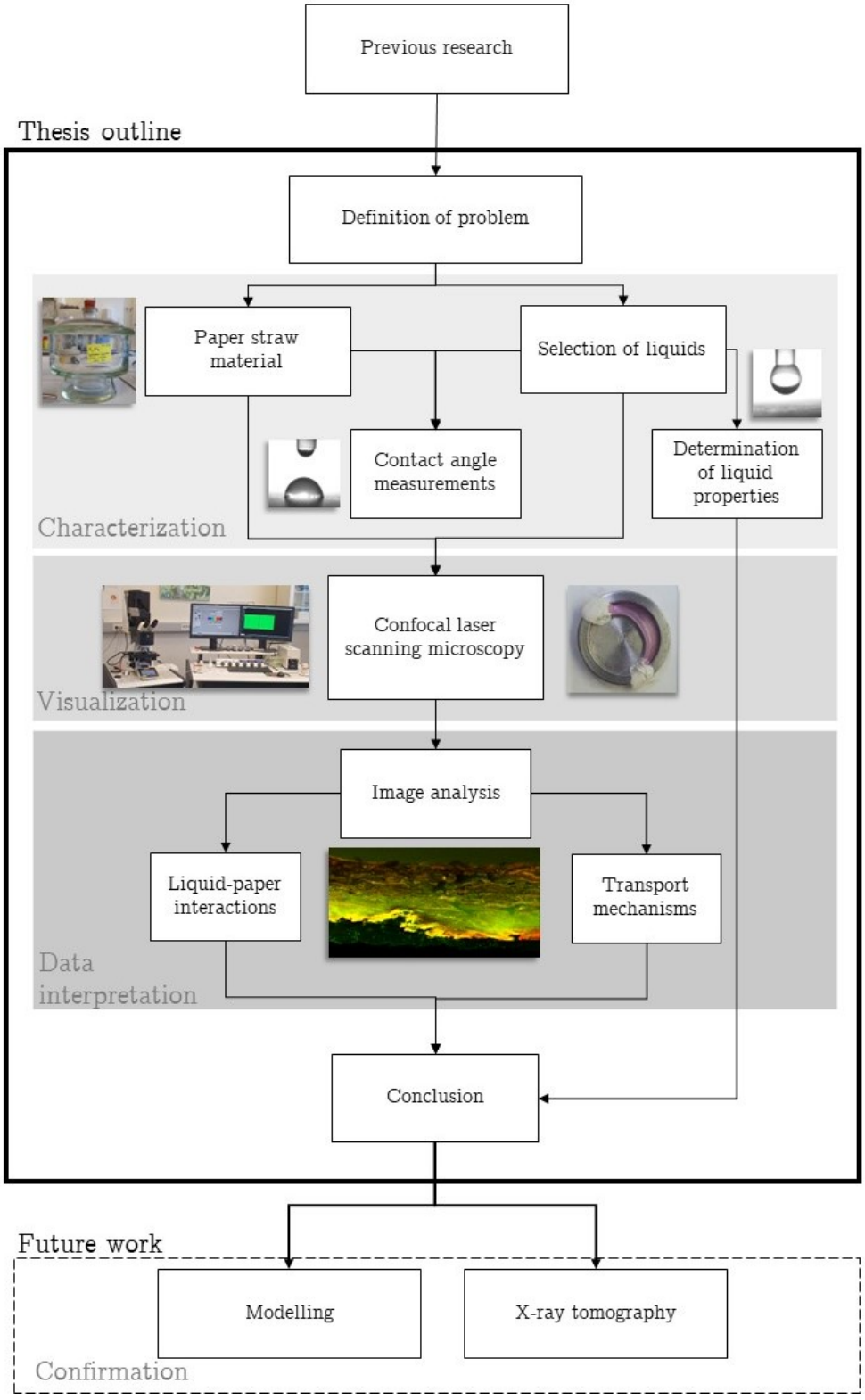

Figure 1.1: *Flowsheet of the thesis outline.*

1.2 Limitations

The main focus of this project is to evaluate the influence of different liquid properties on the penetration depth as a function of time and the interaction with the paper straw material. Considering the time constraints of this project, only one type of paper straw material will be considered. The project will not focus on other materials than the specific paper straw material used in Tetra Pak®'s production and how it interacts with liquids used in the application areas.

The project is limited to characterizing different liquids which are applicable in the production process, the consumer phase and in the recycling process. The liquids will be modified according to one of the following properties, surface tension, viscosity, pH or by addition of saccharose or NaCl. Other properties of which liquids could be modified are not taken into consideration during this project.

Characterization and visualization of paper-liquid interactions will mainly be based on CLSM experiments in combination with image analysis, other techniques will not be evaluated during this project. However, techniques such as viscosity measurements, pH measurements and surface tension measurements will be performed for the characterization of liquid properties and contact angle measurements will work as a complement to understand the liquid interactions with the paper fiber network and the mechanisms occurring.

2
Theory

This section aims to introduce theoretical concepts used throughout the project. Section 2.1 give fundamental theory about the structure of wood. A foundation for the production of paper and its properties as well as the production of paper straws are included in Section 2.2. Further, mass transport mechanisms in paper-based materials are explained in Section 2.3. Section 2.4 explains the fundamentals of the characterisation techniques that can be used to characterize liquids and paper material, and the interaction between them. In Section 2.5, the properties of materials used for liquid modification are presented, together with an associated justification for each choice.

2.1 Structure of wood

Cellulose, which is the structural component of cell walls in plants, is the most abundant renewable bio-polymer on earth [12]. This makes it both cheaper and more accessible than other common bio-polymers. In addition to the low price that cellulose-based materials have, they encounter desired properties like high mechanical strength, low weight, biodegradability and renewability, which make them suitable materials for replacing plastic drinking straws [4].

Cellulose chains are built up of β-1,4-linked anhydro-D-glucose units where every second unit is rotated 80° with respect to its neighbour. Cellulose is characterised as a high molecular weight homopolymer and the degree of polymerisation is commonly up to 20 000, although shorter chains can exist [13]. Cellulose chains do not occur individually, they are assembled in larger crystalline units of 36 cellulose chains called elementary fibrils, which in turn build up micro-fibrils that build up familiar cellulose fibers, forming the hierarchical structure of wood [14, 13]. The cellulose fibers are naturally formed as tubes to enable transport of water inside the tree and the hollow void inside the fiber is called a lumen [15]. Together with cellulose fibers, wood cells are built up by hemicellulose and lignin. Hemicellulose is a carbohydrate polymer while lignin consists of phenylpropane units and acts like a glue between the fibers. Cellulose, hemicellulose and lignin are together ordered in a three-dimensional polymer network, building up the natural composite material wood [16, 17].

2.2 Production of paper straws from wood

Paper is defined as "a thin layer of mostly cellulosic plant fibers, produced on a screen by dewatering a slurry of fibers in water" [18, p. 6]. The production of paper-based drinking straws starts with the production of a slurry from the complex wood raw material, called pulp [19]. Pulp is in turn defined as a suspension of fibers and can be produced by separating the cellulose fibers chemically or mechanically from each other [14]. In chemical pulp production, fiber defibration is based on the dissolution and removal of lignin, which results in yields of 45-50% [19, 17]. Mechanical pulp is instead produced by mechanical separation of the fibrous constituents of wood where the lignin remains in the pulp and is plasticized during the process which gives a higher yield, 80-95% [14, 19]. It is the length of the fibers in the pulp that determines its quality. The fiber length is, in turn, dependent on the wood type used in the pulp production. Typically longer fibers, around 3 mm, are extracted from softwood which belongs to gymnosperms, resulting in a paper with higher strength. Shorter fibers, around 1 mm, are instead extracted from hardwood, which belongs to angiosperms, and enable the production of more uniform paper sheets [14, 15, 20, 19].

A variety of chemicals, fillers and other additives are added to the pulp before being further processed into the final paper product [9]. Fillers, for example mineral particles, are added to the paper for many reasons. They improve the optical properties and the dimensional stability of the paper, can fill voids in the fiber matrix, enhance printability and decrease the roughness of the sheet surface. Fillers can also lower the price of the raw material and therefore create better profitability in paper manufacturing [19]. The manufacturing process, shown in Figure 2.1, includes several different equipments; a headbox, a wire section, a press section, a dryer section, a size press, sometimes but not always a coating station, a calendar and a pope reeler [21].

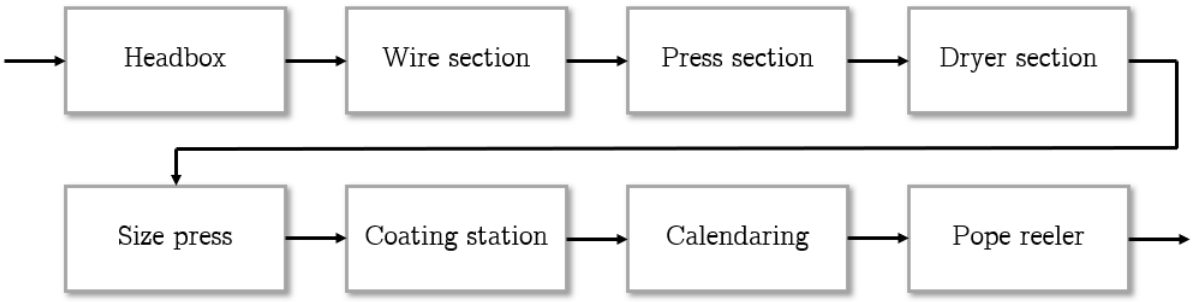

Figure 2.1: *Flowsheet showing the equipment and steps included in the paper manufacturing process.*

The paper manufacturing process starts with loading pulp suspension into the headbox, which allows the pulp suspension to equally distribute in the cross-direction of the machine and enables high uniformity of the suspension. The pulp suspension flows from the headbox into a moving, water-permeable wire section, where dewatering of the suspension takes place, forming a paper web. The wire section prevents

unwanted fiber flocculation and also causes the fibers of different lengths to align more or less in the flow direction by oriented shear [21]. This is the reason why paper has an anisotropic structure when the fibers finally cohere and form a fiber network. The anisotropy of the paper results in different properties along the directional axes, often called machine direction (MD), cross-direction (CD) and thickness direction (ZD) [9, 20]. The different directions of the paper is shown in Figure 2.2.

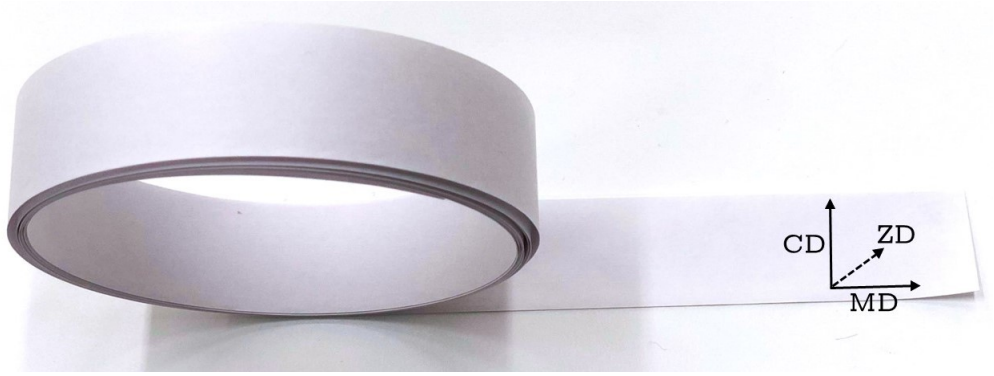

Figure 2.2: *Visualization of the paper straw material and its orientation that arise in the manufacturing process. MD is the machine direction, CD is the cross-direction and ZD is the thickness direction.*

Traditionally a single wire is used in the paper production process. The water drains down through the machine's forming wire which means small fibers, fillers and sizing are lost through one side of the web, giving rise to a distinguishable two-sidedness of the paper. The top side of the paper in the paper machine becomes more smooth and is called the print side (PS) whereas the side where water drains down through the wire becomes rougher and is called reversed side (RS) [22].

The fiber web leaving the wire section still contains 80% water and is therefore entering a press section with the purpose of increasing the dry content of the paper web [21]. This is done by pressing the material together allowing bonds to form between the fibers and thereby increasing the strength of the web [9, 21]. The water content is reduced to 50% in the press section [23]. Following, the paper enters the drying section where the paper is dried by thermal heating to its final moisture content of 2-10% [21]. During the drying, hydrogen bonds are formed between the fibers which give the strength of the paper. Some drying sections in the manufacturing process include a size press where a certain media is applied to the web surface, called sizing [21].

The purpose of sizing is to increase the strength of the paper and/or modify the surface properties to enable control of liquid penetration and liquid uptake in the paper, which are important properties to control for the paper material used in paper-based drinking straws [17, 21]. The sizing is followed by calendering, where the paper web is compressed between two highly-polished rolls with different special properties enabling modification of the surface smoothness of the paper web [22]. The degree of calendering is determined by the requirements of the paper application. The last step

in the paper manufacturing process is the reeling of continuously produced paper, forming paper rolls, and in this step, the paper quality cannot be further improved [21].

2.2.1 Properties of paper

The fibers in paper are held together by hydrogen bonding between hemicellulose and cellulose. Hemicellulose thus increases the strength of the paper while lignin, which does not contribute to hydrogen bonding, decreases the strength of the paper. Since water interferes with the hydrogen bonds, the paper loses much of its strength when it becomes wet. Wood fibres and paper are hygroscopic in their nature, which means that when they are completely dried, they will absorb moisture from the environment [24]. This means that the relative humidity (RH) in the environment affect the paper's moisture content, which also affects the swelling or shrinking of the paper. A higher RH in the surrounding environment makes the fibers swell and a lower RH makes the paper shrink [24, 25]. Since the fibers are bounded to the neighboring fibers, swelling will separate them [25]. An additional important property of paper fibers are their auto-fluorescence which is best excited at 488nm [26].

2.2.2 Production of paper straws

Production of paper straws can in an effective way be done by using paper straw machines. One example of a machine is the Hauni Straw Maker which makes it possible to produce high-quality paper straws in an automated way [27]. The manufacturing process for paper straws is illustrated in Figure 2.3. The paper is inserted into the machine and the paper is cut in half along MD in order to create two equal strips. One of the strips is then brought to a gluing section where one of the sides of the paper is covered with glue, this stripe is then moved forward to an overlapping section where the two strips are joined together with displacements on each side and glue in between them. The combined paper strip is then transferred into the tube forming unit which produces a long paper straw. The paper straw is then chopped into the desired dimensions. By using this method it is possible to produce 300 meters of paper straw per minute [1].

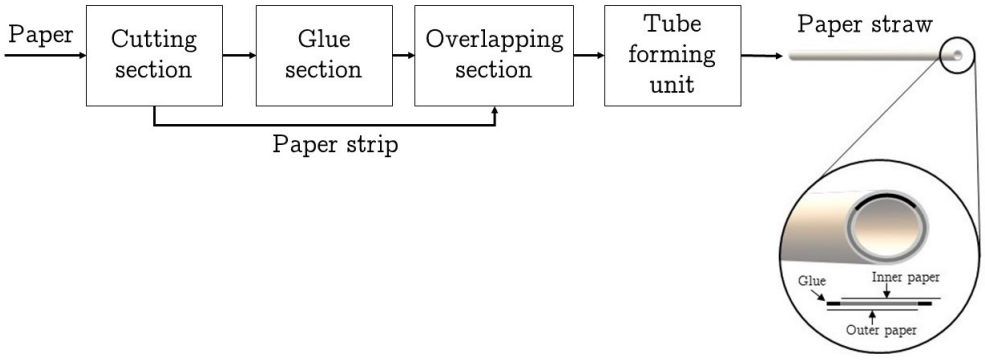

Figure 2.3: *Straw production from paper. Inspiration for image [1].*

2.3 Liquid transport mechanisms in straw material

Paper used in the application of paper straws is, as mentioned in Section 2.2, composed of several cellulose fibers which could consist of different lengths controlled by the specie of the wood. Together the several cellulose fibers compose a porous network. When liquid penetrates into paper material, this network can be divided into three phases; a gas phase, a fiber phase and a water phase. Since the paper straw material is porous, a space between the cellulose fibers exists, called the pore space. The pore space can be utilized by both liquid and air where the air usually consists of water vapour and dry air [28, 29].

One fundamental basis to understand when investigating the interaction between paper straw material and different kinds of liquids is how the liquid penetrates into the material. Generally, the transport mechanisms are divided into three; liquid transport through paper fibers, capillary transport of liquid through pore space (inter-fiber) and vapor diffusion through pore space [30]. The three different transport mechanisms are visualized in Figure 2.4.

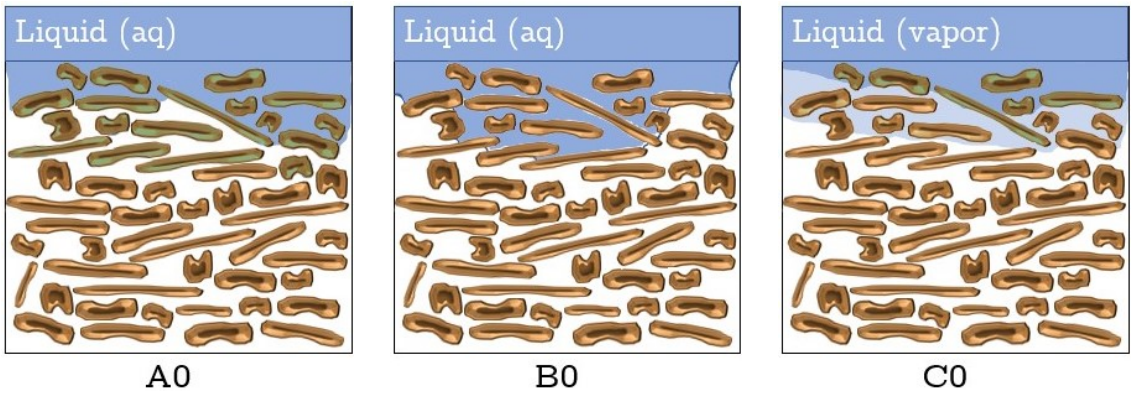

(a) *Liquid transport through paper fibers.*

(b) *Capillary transport of liquid through pore space (Inter-fiber).*

(c) *Vapor diffusion through pore space.*

Figure 2.4: *Visualization of the main three transport mechanisms of liquid through paper straw material.*

In Figure 2.4, the cellulose fibers are brown, the liquid is blue, the pore space is white and the vapor is light blue. Figure 2.4a shows the mechanism when liquid is transported through the paper fibers causing swelling of the fibers. Figure 2.4b shows the capillary transport of the liquid in the pore space and Figure 2.4c shows the liquid vapor diffusion in the pore space which causes the pore space to increase. These mechanisms can appear individually but may also be combined depending on both the paper and liquid material [31].

2.3.1 Moisture sorption isotherm

When working with cellulose products, such as paper straws, the moisture content of the material becomes a key parameter. As mentioned in Section 2.2.1, the moisture

content of a product is affected by the RH and consequently the temperature in the environment. Depending on the moisture content of the paper straw material the mechanical properties are influenced [32]. Previous research has shown that increased RH yield decreased strength of the material [33, 32]. Since the paper straw properties can be affected by fluctuations in the RH and temperature the moisture sorption isotherm becomes important when investigating cellulose products [34].

The moisture sorption isotherm is a relationship between the RH and the moisture content at equilibrium [35]. The process of sorption can be divided into absorption and desorption. The absorption indicates the amount of vapor the cellulose product can collect and desorption is the reversed process, meaning the amount of water which is released as vapor. The moisture sorption isotherm can thus yield information about interactions between non-constant environments and the paper straw material.

2.3.2 Kinetics of liquid transport

The structure of real porous media is complex which makes it hard to model and simplified models are necessary [36]. In 1918, Lucas and Washburn proposed the well-known Lucas-Washburn equation which is a fundamental equation used to describe liquid imbibition through porous media, shown in Equation (2.1) [37].

$$h^2 = t\frac{2\sigma R\cos\theta}{2\mu} \tag{2.1}$$

, where h is the liquid height into the capillaries, t is the time, σ is the vapor surface tension, R is the radius of the cylindrical capillary, θ is the contact angle and μ is the liquid viscosity. This equation is however assuming circular cross-sections of capillaries which is not the case in reality. Furthermore, when fibers absorb liquid it causes them to swell and the porous structure of the substrate is changed, both by changes in the fiber shape and the capillary radius, and hence the permeability and the porosity of the material, which is not taken into consideration in Equation (2.1)[38]. Despite the many limitations of the Lucas-Washburn equation it is commonly used to predict the liquids transport through porous media, such as paper. Researchers have shown by experiments that the penetration depth of liquid into the paper substrate often appears to be linearly proportional to the square root of time. It has also been shown that the RH have an effect on capillary rise, the higher the RH the faster the capillary rise [38].

The measurement of liquid penetration into the ZD of the paper is difficult to do in reality and wicking measurements in the MD and CD can easier be measured [39]. Liquid wicking through paper in these directions has therefore previously been studied more. This has often been done by optical methods, commonly by dipping a paper strip into the liquid and recording the liquid rise in the strip with a camera [38, 40]. The capillary rise in one case was 8mm after 420s in a paper strip with a width of 20mm [38]. Transplanar liquid penetration into single-layer textiles, which are also porous materials, have however been previously studied by a method called demand

wettability method [41]. A liquid source is placed in contact with the single-layer textile and the weight loss of the source is measured. From this study, the absorption of liquid into the textile was approximately linear to time, but it did not provide data about the transport mechanisms occurring [41]. NMR has been used to visualise the liquid transportation of oil into textiles [42], and X-ray radiography has been used to study the transplanar wicking in knitted textiles [43].

2.4 Characterization techniques

A description of theory for characterization techniques used during the project is provided in the following Sections. Section 2.4.1, 2.4.2 and 2.4.3 describes the techniques for characterizing and visualizing the liquids and the paper straw material, as well as their interaction. Section 2.4.4 and 2.4.5 provides an overview of the techniques used to characterize the different liquids.

2.4.1 Confocal Laser Scanning Microscopy

Confocal laser scanning microscopy (CLSM) is an imaging technology which analyzes structural formation processes [2, 44]. In this regard, it provides a tool for monitoring structural changes by using optical sectioning under dynamic conditions under the microscope. The main components of the CLSM can be seen in Figure 2.5.

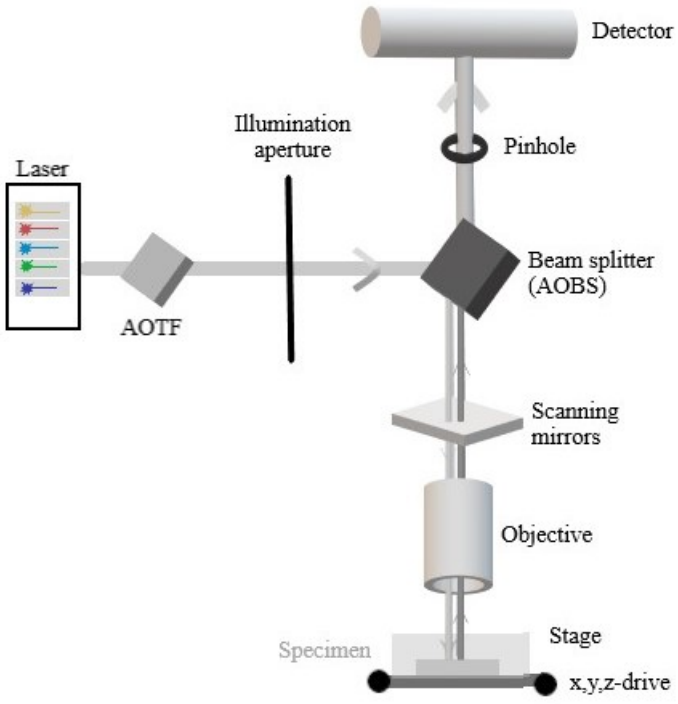

Figure 2.5: *Main components of the CLSM including laser, AOTF, illumination aperture, beam splitter (AOBS), scanning mirrors, objective, stage and specimen. Inspiration for image [2].*

To describe the process, the sample is placed on a stage. The laser light is then turned on and carried through an acousto-optical tunable filter (AOTF). The AOTF controls the laser power and combines the light from the several lasers used. After the AOTF the light is passed through an illumination aperture in order to focus the beam. Next, the beam is passed through an acousto-optic beam splitter (AOBS) where specific wavelengths of the incident laser light are selected to either be reflected or passed through the AOBS depending on which wavelength that is of interest [45, 2]. Once the light has passed through the AOBS the beam is scanned through scanning mirrors. The beam then goes through an objective

which illuminates the sample and collects the re-emitted fluorescent light after interaction with the sample. The primary function of the objective is to establish constructive interference on the focal point as well as target the laser beam. From the objective, the beam again travels through the scanning mirror and the AOBS. The beam is then transferred through a pinhole in order to secure that fluorescence light alone from the focal point in the sample is detected. The pinhole also focuses the beam once again and depending on the signal-to-noise ratio the size of the pinhole is restricted. The light is then entering the detector which collects and counts the number of photons at a specific wavelength and therefore an emission fingerprint is produced [2]. Due to the fact that the CLSM technology can monitor the structural changes in 3D under dynamic conditions, this technique is useful in order to both analyze the interaction between the paper straw material and the liquid and also to analyze the characteristics of the paper straw material.

A prerequisite for CLSM is that the sample needs to be fluorescent, either by auto-fluorescence or by the addition of a dye which is fluorescent. The organic chloride salt Rhodamine B is a commonly used fluorescent dye. Rhodamine B is water soluble and used in many applications such as in paper dye, additive to drugs as well as cosmetics and as colorants in inks. Rhodamine B is a fluorochrome which means that it can induce flourecence in other substances, therefore the salt can be used in order to label compounds which are not originally fluorescent and thereby be visible in for example CLSM [46].

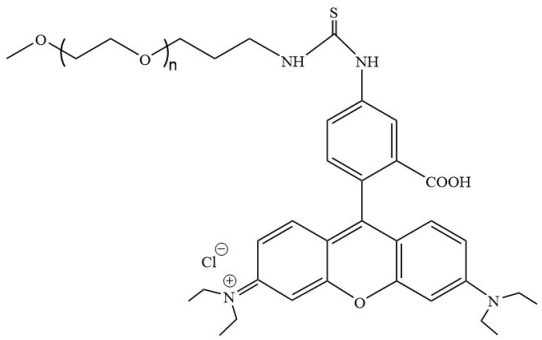

Figure 2.6: *Structural formula of Rhodamine B PEG.*

A monosubstituted Rhodamine B PEG (mPEG-RB) with a molecular weight (M_w) of 1000 could be used as a dye. The advantage of using the substituted Rhodamine B is that it is easier to use with higher stability compared to other substitutions [47]. Since PEG is relatively inert the substitution is of interest. Rhodamine B PEG is fluorescent with maximum excitation wavelength at 544nm. The substitution is as well soluble in water and sensitive to both light and temperature. The structure of the monosubstituted Rhodamine B PEG is visualized in Figure 2.6.

2.4.2 Image analysis

To perform image analysis different software can be used and one example is the open-source software Fiji. The Fiji software is based on the ImageJ2 framework and is used for analyzing, visualizing and validating scientific images [48]. The advantage of using image analysis is that quantitative data can be obtained from qualitative measurements.

2.4.3 Contact angle and surface tension

When a liquid encounters a solid surface it either wets the surface or forms a droplet. The degree of wetting depends both on the surface tension of the liquid and the properties of the surface. To determine these properties the contact angle, θ, can be measured. This can be performed using the optical sessile drop technique where a drop is placed on the substrate, as illustrated in Figure 2.7a, and the contact angle is determined [49]. The contact angle, in turn, is defined as the angle between the liquid-vapor interface and the solid surface, measured from the three-phase contact point, illustrated in Figure 2.7a [50].

(a) *Illustration of the contact angle, θ, between the solid surface and the tangent line of the liquid phase drawn from the three-phase contact point. γ_{SV}, γ_{SL} and γ_{LV} denote the forces acting between the solid, liquid and vapor interfaces.*

(b) *Illustration of surface tension measurement using the pendant droplet method. z, x, s and θ are parameters used to calculate the shape factor β which is needed to determine the surface tension of the liquid. R_0 is the radius of the droplet curvature at the apex. Inspiration for image [51].*

Figure 2.7: *Illustration of contact angle and surface tension measurement methods.*

The surface tension, γ_{LV}, is the tension that causes the liquids to form drops. In the bulk, liquid molecules sense the same amount of cohesive forces in all directions whereas the molecules at the surface experience uneven forces due to the lack of forces in one direction, which is caused by the surface. It is this asymmetry of the cohesive forces at the surface that gives rise to the surface tension [52]. The surface energy, γ_{SV}, is the energy between the solid surface and the vapor whereas the interfacial tension is the tension between the solid and the liquid, γ_{SL}. The reason why a contact angle occurs when a droplet is placed on a solid surface is because of the mechanical equilibrium between the three tensions described above. Young's equation, Equation (2.2), shows the relationship between these three interfacial tensions [53].

$$\gamma_{SV} = \gamma_{SL} + \gamma_{LV} \cdot \cos\theta \tag{2.2}$$

, where γ_{SV} is the surface energy, γ_{SL} is the interfacial tension between the solid and the liquid, γ_{LV} is the surface tension of the liquid and θ is the contact angle.

Young's equation assumes ideal surfaces which are perfectly flat and chemically homogeneous, but this is however not the case for surfaces in reality. Therefore the dynamic contact angle, which is measured as a function of time, is usually determined [54].

The contact angle is used to determine wetting, spreading and absorption of the liquid on a surface. Wettability gives information about if the surface is hydrophilic or hydrophobic in nature. If a hydrophilic liquid gives a contact angle <90°, this indicates good wettability and the material is hydrophilic. A contact angle >90°, with the same hydrophilic liquid, on the other hand, indicates low wettability and that the material is hydrophobic [9]. The wettability is dependent on the surface tension of the liquid and the surface energy of the solid surface, where the surface tension must be lower than the surface energy in order for a liquid to totally wet a surface [55].

It is the balance between the interfacial surface tensions in play that mainly determine if a droplet on a surface will retain its shape or spread over the surface. In addition, the spreading of a liquid on a surface is dependent on the chemical composition of the surface, the surface roughness and the vapour pressure of the liquid [56]. The physics of liquid spreading is complex in paper materials since its porous structure enables liquid absorption and fiber swelling [38]. Liquid imbibition in a porous media is caused by the capillary pressure generating a suction force and the main factor affecting the absorption is the surface tension at the interface of the surface and the liquid. The prerequisite for the liquid to wick up through the pores in the paper is that the adhesive forces, which are the forces binding molecules of different substances together, are greater than the cohesive forces, which are the attractive forces between molecules of the same substance [38, 57]. By analyzing the development of a drop volume and contact angle over time it is possible to obtain information about the absorption of liquid into the substrate [58].

The surface tension of liquids can be determined using the optical pendant drop technique, which is visualized in Figure 2.7b, where a drop of the liquid of interest is pushed out from a tube to a certain volume and the curvature of the drop profile is analyzed [59]. This is a simple method that only requires a tube that the liquid can be pushed through, a camera and a light source [60]. It has been shown that the surface tension can be related to the drop shape by Equation (2.3) [51].

$$\gamma = \frac{\Delta\rho g R_0^2}{\beta} \tag{2.3}$$

, where $\Delta\rho$ is the difference in density between the drop and the surrounding medium, g is the gravitational constant, R_0 is the radius of the droplet curvature at the apex and β is called the shape factor and can be determined by utilizing Young-Laplace equation. The Young-Laplace equation can, in turn, be described through three first-order equations, shown as Equation (2.4), (2.5) and (2.6) [61].

$$\frac{dx}{ds} = \cos\theta \tag{2.4}$$

$$\frac{dz}{ds} = \sin\theta \tag{2.5}$$

$$\frac{d\theta}{ds} = 2 + \beta z - \frac{(\sin\theta)}{x} \tag{2.6}$$

, where z, x, s and θ is shown in Figure 2.7b. Due to this, differences in droplet volume can affect the obtained values for the surface tension when using the optical pendant droplet method since the droplet shape is dependent on volume [61].

2.4.4 Determination of pH

The pH of a solution is a measure of the concentration of hydrogen ions, H^+, present in the solution and pH is a common measurement for the characterization of the acidity of different liquids [62]. Excess of H^+ in a solution makes it acidic while an excess of hydroxide ions, OH^-, in a solution makes it basic [63]. pH can be measured by using either colorimetric methods with indication solution paper or with a more accurate electrochemical method using an electrode, often called a pH meter [62].

Different studies have been done regarding the swelling of cellulose fibers at different pH, but only when the fibers are exposed to different pH in pulp production [64, 65, 66]. It has been shown that maximum swelling of fibers in pulp occur between pH 8 to 10 [64]. Initially, it has been interpreted that the cellulose fibers swell due to dissociations of the OH-groups present along the cellulose molecule [66]. Since it has been shown that the swelling of cellulosic fibers can be affected by pH in the pulp, it is of interest to further investigate the paper-liquid interactions when the pH of the liquid has been modified to either acidic or basic.

2.4.5 Fluid viscosity

Viscosity is a measure of the resistance of matter to deform under a certain force and is an important property when characterizing liquids [67]. The viscoelastic behavior of liquids and semi-solid materials can be determined by a rheometer where the most commonly used type for analyzing food materials and liquids is a rotational rheometer [67]. A rotational rheometer can be used to examine both the viscosity and viscoelastic properties of liquids. Thick and thin liquids can be measured with a cup and bob rotational rheometer [67, 68]. The basic working principle for this setup is that the test liquid is sheared between the surfaces of the cup and the bob, inside the so-called test cell, where the cup is rotating and the bob is fixed, called the Couette principle, while the torque is measured at the rotating surface [69]. The torque has to overcome the viscous force to enable the deformation of the test liquid and is therefore a measure of viscosity [70]. Viscosity measurements give information about flowability and flow parameters, where an increased viscosity decreases the flow rate of the liquid. Flow parameters are essential properties to evaluate since they potentially can affect the mass transport of liquid through the paper [69].

2.5 Materials for liquid modification

In the following sections, the chemicals used for liquid modification are described, together with a motivation for the choice of chemical.

2.5.1 Tween®20

Tween®20, with the trivial name polysorbate 20, has the chemical formula $C_{26}H_{50}O_{10}$ and the chemical structure shown in Figure 2.8.

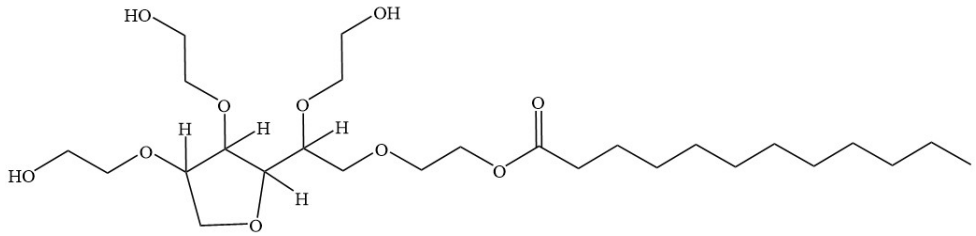

Figure 2.8: *Structural formula of Tween® 20.*

Tween®20 is a non-ionic surfactant commonly used in the pharmaceutical industry or as a food additive. It acts as an emulsifier with the purpose to stabilize the emulsion [71]. Surfactants are amphiphilic in nature with a hydrophilic head group and a hydrophobic tail which gives them the unique property to self-assemble at interfaces, drastically changing the interface's properties. The addition of surfactants to a solution generally lowers the surface tension, already from low concentrations up to the critical micelle concentration (CMC), which is the concentration at which micelles start to form. The surface tension will, however, not change at concentrations above CMC and will thus remain constant [72]. The surfactant adsorption from a solution to the surface-water interface is driven by two factors; the hydrophobic effect and the energy gained from turning the liquid-surface contact into surfactant-surface contact [73].

2.5.2 Polyethylene glycol

Polyethylene glycol (PEG), also called polyoxyethylene, is a semicrystalline, inert and hydrophilic polymer that, due to its biocompatibility, often is used in the biomedical industry [74, 75, 76]. PEG is synthetically synthesised by ring-opening polymerisation of ethylene oxide monomers, whereby different molecular weights can be achieved [76]. The general chemical formula for PEG is displayed in Figure 2.9. Polymers can be added to solutions with the purpose to vary the viscosity. Most polymers show a non-Newtonian behaviour and are often shear thinning, which means that the resistance to deform decreases with an increased shear rate. This is due to the decreasing entanglement

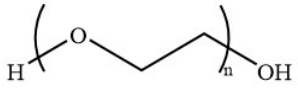

Figure 2.9: *General chemical structural formula of PEG where n is the number of repeating units.*

density upon increasing shear rate, which enables the polymer to easily flow. The viscosity is dependent on the chain length of the polymer, the temperature and the concentration. Longer chains and higher concentrations cause more entanglements between the polymer chains in the solution which causes difficulties for the polymer chains to move and thus increase the viscosity while an increased temperature causes increased free volume and makes it easier for the polymer to move [77].

Polymers can also affect the surface tension of solutions. There are two main ways of action to enable a variation of the surface tension of polymer solutions; either by changing the molecular weight or by changing the solution properties of the polymer [52]. It has been shown that the higher the molecular weight of a PEG solution, the lower the surface tension, which is related to the lower solubility high molecular weights bring due to entropy effects [52]. The surface tension decreases due to poor interaction between the solvent and the polymer which causes the polymer to move to the surface where the polymer-solvent contact points are less than inside the solution [52]. Poor solvent-polymer interaction causes polymer adsorption onto surfaces, but also conformational entropy loss is a driving force for the adsorption of polymers onto surfaces [78].

2.5.3 Electrolytes

In order to customize surface tension or pH different types of electrolytes can be used. According to literature electrolytes should increase surface tension as a function of concentration [52]. Sodium hydroxide which has the molecular formula NaOH is a strong electrolyte and completely dissociates into its ions in solution [79]. Since NaOH is strongly alkaline it can be used to increase the pH of a solution. It has also been shown that NaOH can cause cellulose to swell [80].

Hydrochloric acid is as well as NaOH a strong electrolyte. Hydrochloric acid has the molecular formula HCl and since it is a strong acid which consist of H^+ ions [81]. Since the compound contains H^+ ions, HCl can be used in order to decrease the pH of a solution.

NaCl is the molecular formula for sodium chloride which is commonly also known as table salt [82]. NaCl is a neutral electrolyte which contributes to the conductivity in the solution [83]. In addition to NaCl used in industrial processes, it also plays an important role in the production of paper pulp as well as in many consumer products, due to this NaCl is of interest during this project.

2.5.4 Saccharose

Saccharose, sucrose or table sugar are three synonyms which all represent the product of glucose and fructose units combined together with an acetal oxygen bridge, the chemical structure is visualized in Figure 2.10.

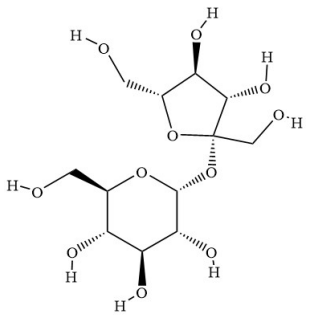

Figure 2.10: *Structural formula of saccharose.*

Saccharose is a white crystalline solid with high solubility in water and is commonly used as a sweetener in consumer products [84]. Since saccharose is used in many consumer products, such as beverages, the interaction between saccharose and paper straw material is of interest. Considering the fact that saccharose as well has shown an increased advancement of the surface tension this compound is of great interest during this study [52].

2.5.5 Yes

Yes original is a mild detergent available for consumer use. Yes is a mixture of sodium laureth sulfate, lauramine oxide and alcohol [85]. The mixture is marked with the globally harmonized system hazard statements H319 and H412. Hazard statement H319 implies that it causes serious eye irritation and H412 that it is harmful to aquatic life with long-lasting effects [86]. The mixture has a pH between 8.7-9.3 and is soluble in water. The GHS statements imply that this is not a common modifier for beverages but is of interest since it contains both anionic surfactants and zwitterionic surfactants. Due to the fact that the substance contains surfactants the mixture could be used to decrease the surface tension of liquids as a function of concentration [52].

3
Methods

The following sections describe the materials and experimental equipment used throughout the project, as well as the methods used to perform all steps. As part of the project, a literature study was conducted. Information and resources were gathered from databases which are considered to be reliable sources.

3.1 Materials

During the project high vacuum grease DOW CORNING®, D(+)-Saccharose (M_w 424.30 g/mol, Millipore), hydrochloric acid (37%, Millipore), polyethylene glycol (average M_w 3000 g/mol, Fluka), polyethylene glycol (average M_w 35000 g/mol, Fluka), potasium sulfate (≥99%, Supleco), Rhodamine B PEG (M_w 1000g/mol, Nancos), sodium chloride (Merck KGaA), sodium hydroxide (≥ 99%, max. 0.02% K, Millipore), sodium hydroxide (Millipore), Tween® 20 (Acros Organics), V2 paper consisting of 30-50% hardwood and 50-70% softwood, Yes manual dish washing detergent (P&G) was used. Milli-Q® water (Millipore) filtered through a Millipak® express filter (Milli-Q) was used throughout the project.

3.2 Methodology

This section aims to describe the experimental work conducted in the thesis. Section 3.2.1 describes the sample preparation for the CLSM experiments. The CLSM experiments are described in Section 3.2.2. Section 3.2.3 describe how the image analysis was performed. Sections 3.2.4-3.2.6 explains the methodology for the characterization experiments.

3.2.1 Sample preparation

This section aims to describe the sample preparation carried out in the project.

3.2.1.1 Preparation of paper samples for CLSM experiments

In order to perform CLSM experiments the straw paper was prepared in the following way. The paper straw material was cut into small rectangular pieces with the following dimensions, length 1.5 cm and width 2 mm, using a microtome blade. The paper samples were always prepared by cutting on the RS of the paper and in CD. The paper

samples were then placed in a metal cup with a sticky tape in the bottom, the setup is shown in Figure 3.1.

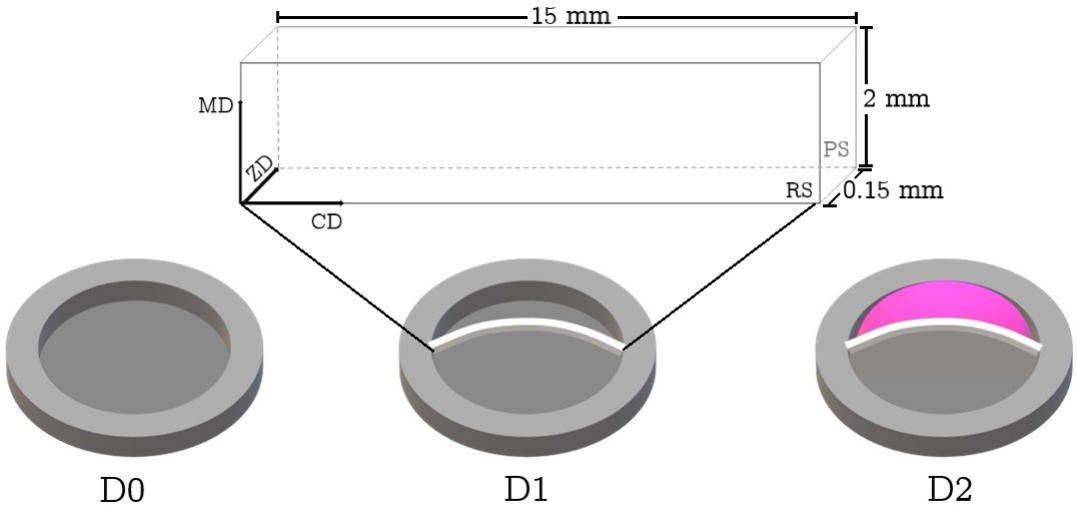

Figure 3.1: *Visualization of sample preparation for CLSM experiments. D0 displays the metal cup, D1 the metal cup with the paper piece in white in the desired dimensions as well as the orientation of the paper in the cup and D2 visualizes the cup with the paper piece and where the liquid in pink was placed.*

3.2.1.2 Conditioning of paper

To evaluate if RH influences the shrinking or swelling behavior in the paper, straw paper exposed to different climate conditions were evaluated. Three different conditions were evaluated and are displayed in Table 3.1.

Table 3.1: *Conditions with corresponding temperature and method used to obtain the desired relative humidity.*

Relative humidity [%]	**Temperature [°C]**	**Method used**	**Salt**	**m_{salt} [g]**
8-9	20	Saturated salt solution	NaOH	11.10
50	23	Climate room	-	-
95	20	Saturated salt solution	K_2SO_4	3.42

The condition with RH of 50% was obtained by placing prepared paper samples according to Section 3.2.1.1 in a climate room. The RH of 8% and 95% were achieved by the following procedure. A saturated salt solution was created by mixing 30 ml of distilled water with the desirable salt for the corresponding RH in a crystallizing dish, the amount of salt added is shown in Table 3.1. The mixture in the crystallizing dish was then positioned in a glass desiccator with a diameter of 15 cm at the lower desiccator plate. The paper pieces were prepared according to Section 3.2.1.1. The metal cup with the paper piece was then together with a data logger of model Tinytag View 2 (Intab, Sweden) or Tinytag Plus 2 (Intab, Sweden) placed on the upper desiccator

plate. The desiccator was then sealed using the lid and grease rim. The paper pieces were stored in the desiccators for at least two days before measurement using CLSM.

3.2.1.3 Preparation of liquid solutions for CLSM experiments

Milli-Q® water was used throughout the project which means whenever water is written in the report, it refers to Milli-Q® water. During the preparations of all liquids, an analytical balance of model Balance XS204 (Mettler Toledo, Switzerland) was used. A stock solution with water and Rhodamine B PEG with a concentration of 100 μM was prepared. The stock solution was used as the source of Rhodamine B PEG in all of the liquids prepared. The following liquid solutions were prepared with a final concentration of 50 μM Rhodamine B PEG in a total volume of 5 ml, and the concentrations of the modifying agents are presented in Table 3.2.

Table 3.2: *Concentrations of liquid solutions prepared for the CLSM measurements.*

Liquid	**Concentration of modifier**
Water	-
Water (mPEG-RB)	50 μM
PEG 3000	11.50wt%
PEG 35000	11.50wt%
pH 2	0.01 M
pH 9	0.10 mM
Tween® 20 (<CMC)	0.04 mM
Tween® 20 (>CMC)	0.08 mM
Yes 0.1wt%	0.10wt%
Yes 0.05wt%	0.05wt%
Yes 0.01wt%	0.01wt%
Saccharose	10wt%
NaCl	60.00 mM

In the following sections, the preparation procedure, the chemicals used and the corresponding motivation for the liquids are described. After the preparation of the liquids in Table 3.2, all volumetric flasks and beakers were properly sealed, wrapped in aluminum foil to avoid light exposure, and put in a refrigerator holding a temperature of +6.8°C to prevent Rhodamine B PEG from breaking down.

3.2.1.3.1 Reference liquid A reference liquid with a concentration of 50 μM Rhodamine B PEG was prepared by mixing 2.5 ml water and 2.5 ml stock solution in a volumetric flask. The reference liquid will further be referred to as water(mPRG-RB).

3.2.1.3.2 Viscosity increasing modifier Two liquid solutions containing 11.5wt% PEG 3000 respectively PEG 35000 were used to increase the viscosity of the liquids with the purpose to mimic more viscous drinks and at the same time keeping the polymers dissolved in the water. PEG is an inert polymer which also was desired to avoid additional interactions with the paper. The polymer solution with PEG 3000 (average M_w = 3000 g/mol) was made by first mixing 10 g water with 3 g PEG 3000.

This was followed by mixing 2.5 ml of the polymer solution with 2.5 ml of the stock solution in a volumetric flask, giving a PEG 3000-Rhodamine B PEG solution containing 11.5wt% PEG 3000. The same procedure was repeated for the preparation of the liquid solution containing PEG 35000 (average $M_w = 35\,000$ g/mol).

3.2.1.3.3 pH changing modifiers A liquid solution with a pH of 2 was made to mimic the pH of orange juice and Coke and a liquid solution with a pH of 9 was used as a complement to see if the liquid transport in the paper differed from the acidic solution, but also since recycling liquids often have a basic pH [87, 88].

The solution with a pH of 2 was made by first mixing 50 µl of a 1 M solution of HCl with 2.45 ml water. 2.5 ml of the HCl solution was mixed with 2.5 ml of the stock solution in a volumetric flask, giving a HCl-Rhodamine B PEG solution with a pH approximately of 2. The solution with a pH of 9 was made by first mixing 40 µl of a 0.1 M NaOH solution with 19.96 ml water. 2.5 ml of the NaOH solution was mixed with 2.5 ml of the stock solution in a beaker, giving a NaOH-Rhodamine B PEG solution with a pH approximately of 9.

3.2.1.3.4 Emulsifier as modifier Liquids containing Tween®20 was used to mimic emulsifiers that sometimes are added in drinks that are usually drunk with straws, for example, milkshakes [89]. The concentrations were chosen to be above and below the CMC, which is 0.06 mM, to examine two different concentrations and how the liquid transport was affected of those.

The solution with Tween®20 (>CMC) was made by first mixing 19.6 mg Tween®20 with 100 ml water to a concentration of 0.16 mM. 2.5 ml of the Tween®20 solution was mixed with 2.5 ml of the stock solution in a volumetric flask, giving a Tween®20-Rhodamine B PEG solution with a concentration above CMC, 0.08 mM. The same procedure was followed when preparing the Tween®20 (<CMC), but with 9.8 mg of Tween®20 added in the first step, resulting in a concentration below CMC, 0.04 mM.

3.2.1.3.5 Surface tension decreasing modifiers Yes was used as an extreme to see the effect of decreased surface tension of the liquids. A dilution series with different concentrations of Yes was prepared in order to determine the differences in liquid penetration rate into the paper straw material. The dilution series with water and Yes was first prepared with concentrations of 40wt%, 10wt%, 1wt%, 0.2wt% and 0.1wt%. 2.5 ml from each concentration in the dilution series was mixed in separate beakers with 2.5 ml of the stock solution, giving a series with Yes concentrations of 20wt%, 5wt%, 0.1wt%, 0.05wt% and 0.01wt%.

3.2.1.3.6 NaCl and saccharose as modifiers A salt solution was prepared to mimic regular rehydration therapy drinks which contain salt [90]. The solution was made by first preparing a water and NaCl solution with a concentration of 120 mM from which 2.5 ml was mixed with 2.5 ml of the stock solution in a volumetric flask, giving a NaCl-Rhodamine B PEG solution with a concentration of 60 mM NaCl.

A sugar solution with a concentration of 10wt% saccharose was prepared since it is the amount of sugar in Coca-Cola which is a common soft drink [91]. The solution was made by first preparing a water and saccharose solution with a concentration of 20 wt% from which 2.5 ml was mixed with 2.5 ml of the stock solution in a volumetric flask, giving a saccharose-Rhodamine B PEG solution with the concentration 10wt% saccharose.

3.2.1.4 Preparation of liquid solutions for viscosity, surface tension and contact angle measurements

Liquids corresponding to those prepared for the CLSM measurements with the same concentrations of the modifiers as presented in Table 3.2 were prepared for the measurements of viscosity, surface tension and contact angle. The difference was, however, that they were made in larger volumes, 25 ml respective 50 ml, and did not contain Rhodamine B PEG. The reason for this was that larger volumes were needed for the measurements and that the low concentration of 50 µM Rhodamine B PEG was assumed to not affect the viscosity, the surface tension and the contact angle. However, if contrary to the assumption Rhodamine B PEG would have an impact, it would affect the liquids only slightly and equally for all liquids.

3.2.2 CLSM experiments

A Leica TCS SP5 II AOBS Confocal (Leica Microsystems, Germany) CLSM equipped with a Lecia DM5000CS microscope (Leica Microsystems, Germany) and an HC PL APO objective with 10x magnification and numerical apparature of 0.40 was used to carry out time-lapse recordings of both the straw paper cross-section thickness change and liquid penetration into the straw paper, the experimental equipment is shown in Figure 3.2.

Figure 3.2: *CLSM instrument. (1) is the microscope, (2) is the objective, (3) shows the sample setup and (4) is the monitoring screen.*

For both recordings, an argon laser excited at 488 nm was used as a light source and

for the liquid penetration studies an additional helium-neon laser excited at 594 nm was used. The emitted signals from the CLSM were recorded in the wavelength interval of 500-550nm for the argon laser and 605-700nm for the helium-neon laser. The time-lapse recordings for the straw paper cross-section thickness change was carried out in the following way. The sample prepared according to Section 3.2.1.1 was removed from the conditioned environment and directly placed on the specimen stage on the CLSM instrument. The time-lapse recording was initiated and images were acquired at 3s intervals, the total measurement time was 3600s. In order to track the changes of RH and temperature in the measurement room a data logger of model Tinytag View 2 (Intab, Sweden) was placed beside the CLSM instrument. The obtained data was analyzed using the image analysis technique in Section 3.2.3.

The time-lapse recordings of the liquid penetration into straw paper was carried out through the following procedure. The prepared sample, described in Section 3.2.1.1, was placed in a climate room with 23°C and 50% RH. The samples were kept in the climate room for at least 24h before measurement with the CLSM. The sample was placed on the specimen stage in the CLSM and time-lapse recording was initiated, images were acquired at 3s intervals. Immediately after the recording was initiated the liquid was introduced onto PS of the straw material, a visualization of this can be seen in D2 in Figure 3.1. The liquid penetration from PS to RS in ZD could thereby be recorded. The total measurement time for these experiment was 1200s. The obtained data was analyzed using the image analysis technique in Section 3.2.3.

3.2.3 Image analysis

The obtained results from the CLSM measurements were analyzed using image analysis and the software Fiji, version 2.3 (National Institutes of Health, USA) [92]. To obtain quantitative results from the time-lapsed recorded images, the following times were analyzed, 6, 12, 21, 30, 60, 120, 300, 600, 900 and 1200s. The additional times 2400s and 3600s were analyzed for the cross-section thickness change measurements. For each time, the images were exported from LAS X Office 2023 version 1.4.4.26810 (Leica Microsystems, Germany) and imported into the Fiji software. The imported image was then modified using the Fiji analyzing tool *grid*, which created a grid of white lines with the area per point of 10 000 pixels^2. Based on the grid created, six analyzing lines can be drawn for each measurement. An example of two modified images from the time-lapse recording is shown in Figure 3.3.

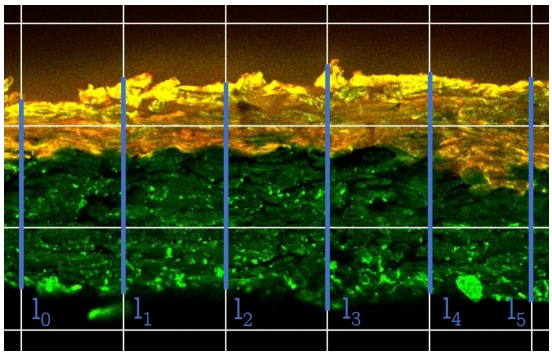

(a) *Cross-section of straw material with outlined measurement lines (blue)* l_0, l_1, l_2, l_3, l_4, l_5.

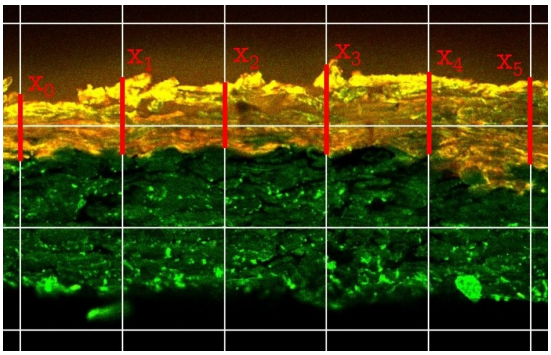

(b) *Penetration depth of liquid into straw material with outlined measurement lines (red)* x_0, x_1, x_2, x_3, x_4, x_5.

Figure 3.3: *Experimental images from CLSM experiments showing how the image analysis was performed using Fiji.*

The cross-section thickness, l, of the straw paper at each vertical grid line was measured and six lengths in µm were obtained, visualized in Figure 3.3a. In order to calculate the mean cross-section thickness ($\bar{l}_t$) at the specific time, Equation (3.1) was applied to the obtained lengths. This procedure was then repeated for all times and replicates.

$$\bar{l}_t = \frac{\Sigma l_n}{n} \tag{3.1}$$

,where $\bar{l}_t$ is the mean cross-section thickness in µm at time t, l_n is the cross-section thickness in µm at the n:th grid line and n is the number of measurement lines. To obtain qualitative data from the time-lapse recordings of the liquid penetration into straw paper the liquid penetration depth, x, was analyzed using the same procedure as for the cross-section thickness, l, and is visualized in Figure 3.3b. The mean liquid penetration depth ($\bar{x}_t$) is calculated using Equation (3.2).

$$\bar{x}_t = \frac{\Sigma x_n}{n} \tag{3.2}$$

,where $\bar{x}_t$ is the mean penetration depth in µm at time t, x_n is the penetration depth in µm at the n:th grid line and n is the number of measurement lines. Since multiple replicates were performed, the calculated mean values $\bar{l}_t$ and $\bar{x}_t$ were adapted to all replicates by calculating the mean value between the replicates at time t, Equation (3.3) show the calculation for the cross-section thickness. Equation (3.3) also applies for the penetration depth.

$$\bar{l}_T = \frac{\Sigma \bar{l}_t}{N} \tag{3.3}$$

, where $\bar{l}_T$ is the mean cross-section thickness between the replicates at time t and N is the number of replicates. Since several replicates were merged together, the standard error for the time t where calculated according to Equation (3.4).

$$\text{SE}\ (\bar{l}_T) = \frac{\sqrt{\frac{\Sigma(l-\bar{l})^2}{n-1}}}{\sqrt{N}} \tag{3.4}$$

, where SE($\bar{l}_T$) is the standard error for the mean cross-section thickness at time t, the numerator is the standard deviation for the measurement lines showed in Figure 3.3. Both the mean values $\bar{l}_T$, $\bar{x}_T$ and the standard errors SE($\bar{l}_T$) and SE($\bar{x}_T$) were then imported to MATLAB® R2022b (Mathworks, USA) and graphs of both the straw paper cross-section volume change as a function of time and the liquid penetration into straw paper as a function of time were created.

3.2.4 pH measurements

A pH meter of model pHenomenal® pH 1100L (VWR, Avantor, USA) equipped with a glass pH electrode with a built-in 221 temperature sensor was used to determine the pH of all the liquid solutions presented in Table 3.2. pH was measured for water and water(mPEG-RB) to ascertain the pH-changing effect of Rhodamine B PEG in all solutions. The pH meter was calibrated prior to use to ensure the quality and reliability of the results. After calibration, the pH electrode was rinsed off with distilled water and put into the liquid until it covered the entire pH electrode. The results were shown on the screen of the pH meter and noted. The procedure was repeated for all liquids.

3.2.5 Viscosity measurements

The viscosity was measured for each liquid presented in Table 3.2 but without the addition of Rhodamine B PEG. The measurements were performed using a rheometer of model ARES-G2 rotational rheometer (TA instruments, UK) equipped with a bob-and-cup geometry consisting of a KIT APS 27.7 mm DIN bob and a KIT APS 30 mm AL cup in stainless steel, the setup is shown in Figure 3.4. The bob-and-cup geometry was used since the liquids were relatively thin. The settings were adjusted as follows; the temperature was set to 20°C and the temperature setting time was 1 min, the viscosity was measured at 24 different shear rates varied between 200 s^{-1} to 1.01 s^{-1}, points per decade were set to 10 and the tolerance was set to 5%. 23 ml of the liquid was provided into the cup after which the bob was lowered into the liquid, as far down so that the liquid covered the entire bob. During the first minute of the measurement, the temperature of the liquid was adjusted to 20°C, after which the bob rotation was initiated. The data from the viscosity measurements from ARES-G2 was generated in Trios software version 5.5.0.323 (TA instruments, UK). The procedure was consequently repeated for all liquids.

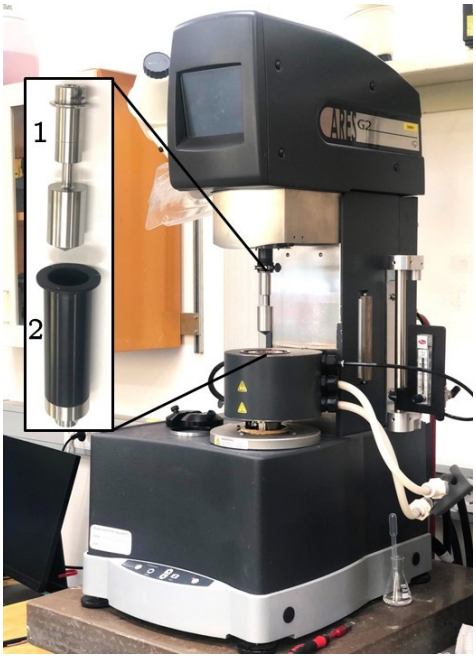

Figure 3.4: *Rotational rheometer. (1) is the bob and (2) is the cup.*

3.2.6 Surface tension and contact angle measurements

The surface tension was measured for the liquids presented in Table 3.2, but without the addition of Rhodamine B PEG, and the contact angle was measured on the same liquids in contact with the paper straw material. Both measurements were performed by a portable goniometer of model Fibro PGX+ Pocket Goniometer (TQC Sheen, Netherlands). All liquids were considered to be similar to water, therefore the settings used during all the surface tension and contact angle measurements were based on the density of water. The device was calibrated prior to use according to the instructions. After calibration, the liquid was loaded into a 1 ml syringe and fed manually into the device through a PTFE tubing, with an outer diameter of 1.5 mm and an inner diameter of 0.2 mm (TQC Sheen, Netherlands), into the goniometer.

When measuring the surface tension a desired volume of 5 µl was manually pressed out of the syringe through the tubing to a hanging droplet, and the measurement was initiated. The surface tension measurements were replicated 5 times for each liquid and the values obtained from the analyzes were tabulated in the software The PacketGoniometer ® version 4.2.6.9 (TQC Sheen, Netherlands).

When measuring the contact angle a volume estimated to 5 µl was manually pressed out of the syringe through the tubing, to a hanging droplet, which was automatically pushed down onto the paper by the device when the measurement was initiated. Images were taken by the device for 5 seconds with an imaging capture rate of 80 frames/s and were shown in the software The PacketGoniometer ® version 4.2.6.9. The baseline for the liquid drop was afterwards adjusted in the image when necessary. Values for the contact angles were tabulated in the software and the contact angle at 0.5 seconds was noted for all liquids. The contact angles for the liquids containing Yes was noted at an additional time point, at 5.0s, to observe the spreading and absorption of the liquid. For each liquid, five replicates were done to ensure the reliability of the measurements.

The procedure of the surface tension measurements and contact angle measurements was repeated for all liquids and the syringe and tubing were properly rinsed through with water between measurements of different liquids.

4

Results & Discussion

This section presents the results obtained from the experiments regarding paper properties before exposure to liquids in Section 4.1, determination of liquids in Section 4.2, swelling and penetration of liquids into straw paper in Section 4.3 and liquid transport mechanisms in Section 4.4.

4.1 Paper properties before exposure to liquids

As mentioned in Section 2.2 the fibers in the paper straw material is oriented in different directions as a result from the manufacturing process. In order to determine whether the anisotropy can be visualized along the directional axes, the paper straw material was analyzed using CLSM. Mentioned in Section 2.2 was the two-sidedness of the paper, abbreviated PS and RS. To evaluate if these two sides are distinguishable on µm-scale, PS and RS where analyzed using CLSM and the result is visualized in Figure 4.1.

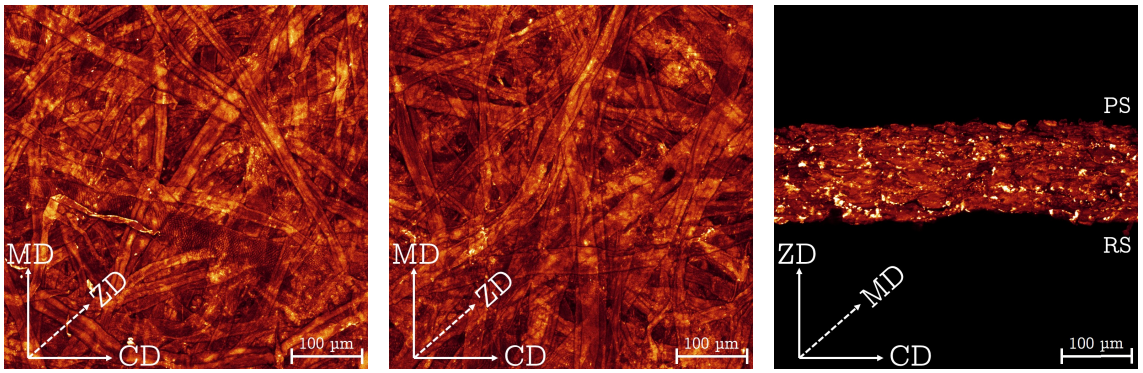

(a) *PS of straw paper.* **(b)** RS of straw paper. **(c)** *Cross-section of straw paper.*

Figure 4.1: *Maximum intensity projections from CLSM experiments showing PS, RS and the cross-section of paper straw material and the corresponding orientation for each case.*

Figure 4.1 displays both MD and CD and at first sight, the two sides exhibit to be similar to each other. Both PS and RS show distinctly connected paper fibers which are anisotropically located. In Figure 4.1c bright dots can be seen throughout the cross-section which possibly could be filler material. The filler material is probably

kaolin clay which is a common mineral used as filler material in paper [93]. Since kaolin clay has a crystal structure the mineral might reflect the laser light in the CLSM and therefore exhibit as bright dots in the maximum intensity projection [94].

According to Section 2.2, PS and RS should differ in the content of fillers. RS should contain less fillers and Figure 4.1a should show more bright dots compared to Figure 4.1b. When observing Figure 4.1b the possible kaolin clay dots also appear and no significant difference between PS and RS can be seen in this aspect. However, when observing Figure 4.1c, RS seems to have a higher extent of bright dots. In order to determine if the filler material is more frequently apparent on PS or RS further investigation is required.

4.1.1 Influence of relative humidity

According to Section 3.2.1.2 the desired RH for the conditioning of the paper straw material was 8-9%, 50% and 95%. Since the RH of 50% was obtained using a climate room this RH is accurate. The RH obtained using saturated salt solutions in desiccators yielded the RH of 8% and 99%, the following results therefore applies for the RH 8%, 50% and 99%. To evaluate the hygroscopic nature of paper and the effects of variations in RH i.e. hygroexpansion, the paper was conditioned at RH 8%, 50% and 99%, and the results are shown in Figure 4.2.

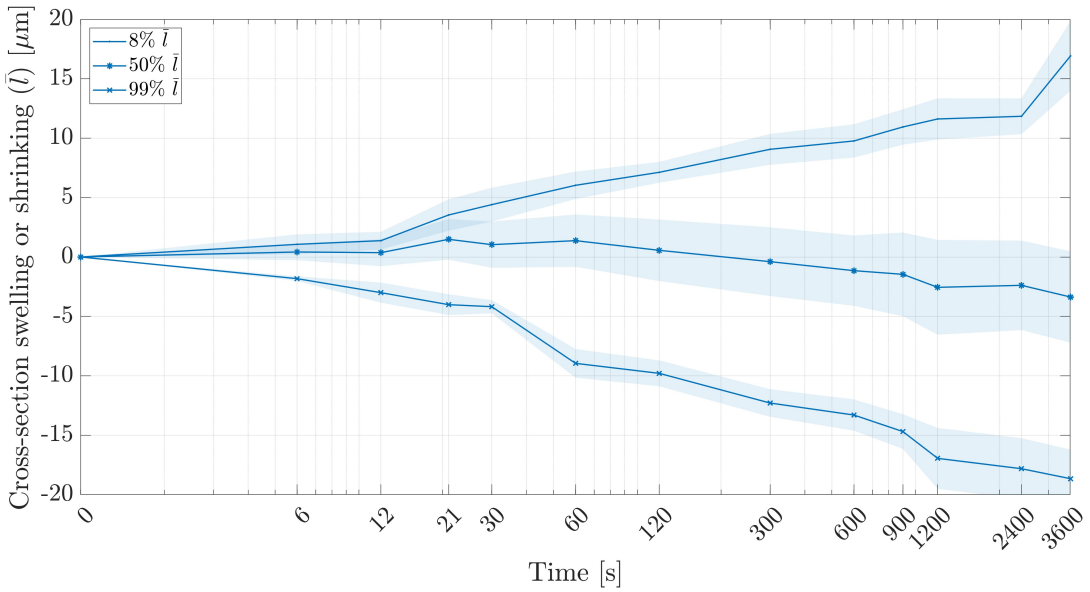

Figure 4.2: *Cross-section swelling or shrinking for conditioned paper straw material in RH 8%, 50% and 99% as a function of time.*

Figure 4.2 displays the swelling and shrinking of the paper cross-section as a function of time in a logarithmic scale on the x-axis. The lines represent the changes in cross-section thickness and the shaded areas next to the lines represent the standard error between the replicate measurements performed for each RH condition. An initial variation in the cross-section thickness was observed between the replicates, and in order to simplify the comparison between the conditions all measurements

were subtracted with the initial cross-section thickness, due to this the experiments start at zero on the y-axis in Figure 4.2.

As mentioned in Section 2.3.1 the moisture content is affected by both the temperature and RH in the environment which is confirmed by Figure 4.2. Even though all measurements for the conditioning experiments were conducted during one day to minimize effects from the fluctuations in the environment, a data logger proved that the RH varied between 11.6-28.2% and the temperature between 21.5-24.5 °C throughout the day. This might have affected the results obtained.

It can be seen that the cross-section of the paper conditioned in a RH of 8% was swelling as a function of time, while the cross-section of the paper conditioned in a RH of 99% showed a shrinking behaviour with time. The cross-section of the paper conditioned in 50% RH on the other hand showed a slight swelling during the first 60s, whereafter the cross-section started to shrink. As seen in Figure 4.2 the total cross-section swelling of the paper stored in the RH 8% was 17 μm corresponding to an increase of 11%. The total cross-section shrinkage of the paper stored in the RH of 50% was 4 μm corresponding to 2% and 18 μm for the paper that was conditioned in the RH of 99% which corresponds to 11%.

4.2 Determination of liquid properties

The liquids used in this project were characterized with respect to the liquid properties pH, viscosity, density, and surface tension as described in Section 3.2.4, 3.2.5 and 3.2.6, and the results are presented in Table 4.1.

Table 4.1: *Properties determined for the modified liquids.*

Liquid	**pH**	**Viscosity [10^{-3} Pa·s]**	**Density [g/cm^3]**	**Surface tension [mN/m]**
Water	5.92	0.98	0.997	30.51
Water (mPEG-RB)	5.52	1.05	-	28.08
PEG 3000	5.11	4.53	1.022	26.92
PEG 35000	5.37	126.55	1.020	30.55
pH 2	2.14	1.02	1.009	31.80
pH 9	9.19	1.01	0.997	34.50
Tween® 20 (<CMC)	5.31	1.00	0.997	29.20
Tween® 20 (>CMC)	5.12	1.00	0.997	27.86
Yes 0.1wt%	7.32	1.10	0.997	24.33
Yes 0.05wt%	7.34	1.03	0.997	24.41
Yes 0.01wt%	6.27	0.99	0.997	31.63
Saccharose	5.96	1.40	1.054	26.60
NaCl	6.74	0.98	1.001	30.86

The two concentrations of 20wt% respectively 5wt% Yes was too high for the CLSM method used in this project since the liquid was penetrating throughout the cross-section of the paper material faster than the CLSM time-lapse recording. Therefore these concentrations are not discussed further, but pH and viscosity was measured and are presented in Appendix A.1.

When comparing the properties of water and water(mPEG-RB) in Table 4.1 it can be seen that water has a higher pH and surface tension but a lower viscosity than water(mPEG-RB). This means that the addition of Rhodamine B PEG in the modified liquids lowers the pH and the surface tension, and increases the viscosity slightly. However, since Rhodamine B PEG is added in the same concentration in all modified liquids it affects these parameters to an equal extent. Since pH was measured for the modified solutions containing Rhodamine B PEG, as described in Section 3.2.4, the pH of the modified liquids should be compared with water(mPEG-RB).

The viscosity and the surface tension was, however, measured for the modified solutions without the addition of Rhodamine B PEG, as described in Section 3.2.5 and 3.2.6, and these properties should therefore be compared with the properties for water. The density for water (mPEG-RB) is missing in Table 4.1 and the reason for this is a lack of information regarding the density of solid Rhodamine B PEG by the retailer [47]. Since the density of solid Rhodamine B PEG is unknown, the density of water(mPEG-RB) was approximated to the density of water since the concentration of added Rhodamine B PEG was negligible in relation to the total volume. Therefore the density of the modified liquids presented in Table 4.1 is calculated with the same approximation since they all contain Rhodamine B PEG, and the calculations can be seen in Section A.1 in Appendix A.

4.2.1 Evaluation of pH

Table 4.1 shows that the five modified liquids PEG 3000, PEG 35000, pH 2, Tween®20 (<CMC) and Tween®20 (>CMC) have lower pH than water(mPEG-RB), which means they are more acidic and have a higher concentration of H^+ ions. The remaining modified liquids pH 9, Yes 0.1 wt%, Yes 0.05 wt%, Yes 0.01 wt%, saccharose and NaCl have a higher pH than water (mPEG-RB), which means they are more basic and have higher concentrations of hydroxide ions, OH^-.

4.2.2 Evaluation of viscosity

When observing Table 4.1 it can be seen that all the modified liquids, except the liquid containing NaCl, have a higher viscosity than water. PEG 3000 and PEG 35000 have the most pronounced effect on increasing the viscosity, which was expected and the purpose of using the polymers as modifiers. PEG 35000 show a significantly higher viscosity than PEG 3000 which agrees with the theory where it is stated that higher molecular weight polymers give higher viscosity, described in Section 2.5.2.

4.2.3 Evaluation of density

When looking at the density in Table 4.1, it can be seen that the liquids with pH 9, Tween®20 (<CMC), Tween®20 (>CMC) and the solutions containing Yes have the same density as water while the liquids with PEG 3000, PEG 35000, pH 2, saccharose and NaCl have slightly higher density. Due to the fact that the modified liquids mostly consist of water, the density of the modified liquids is equal to the density of water. Furthermore, the density for most of the modifying agents is quite similar to the density of water itself, presented in Appendix A in Table A.3.

4.2.4 Evaluation of surface tension

Table 4.1 shows that the liquids PEG 3000, Tween®20 (<CMC), Tween®20 (>CMC), Yes 0.1wt%, Yes 0.05wt% and saccharose have a lower surface tension than water while the remaining liquids PEG 35000, pH 2, pH 9, Yes 0.01wt% and NaCl have a higher surface tension than water. As mentioned in Section 2.5.1 and 2.5.2, emulsifiers, surfactants and polymers lower the surface tension of liquids which explains the behaviour observed for the liquids with PEG 3000, Tween®20 (<CMC), Tween®20 (>CMC), Yes 0.1wt% and Yes 0.05wt%. PEG 35000 and Yes 0.01wt% show an opposite effect and increase the surface tension. This contradicts what previously has been shown in the literature presented in Section 2.5.1 and 2.5.2. As described in Section 3.2.6, the settings used for the surface tension measurements were based on the density of water and since PEG 35000 has the most significant viscosity difference compared to water this can be the reason why PEG 35000 shows another behavior than expected. The liquid Yes 0.01wt% have a low concentration, which explains why the surface tension is close to that of water, but it should however not increase the surface tension since it contains surfactants and the reason for showing this behavior is probably due to measurement errors. Electrolytes should increase the surface tension of liquids as presented in Section 2.5.3 which explains why NaCl, pH 2 and pH 9 have a higher surface tension than water. To visualize the appearance of the surface tension measurements the two extremes, pH 9 and Yes 0.1wt% are shown in Figure 4.3. Figure 4.3 displays a clear difference in the drop shape of the two liquids, which is a consequence of the difference in surface tension.

(a) *Surface tension measurement of pH 9.*

(b) *Surface tension measurement of Yes 0.1 wt%.*

Figure 4.3: *Images showing one replicate of each extreme from the measured surface tension of the liquids.*

4.2.5 Wettability of liquids on straw paper

Determination of the contact angle was done by measuring the contact angle between the paper straw material and the liquid as explained in Section 3.2.6. The contact angle was determined at 0.5 seconds for each liquid, this was due to the fact that bouncing effects of the droplet at that time were negligible. For all the modified liquids five replicates were performed for each liquid in order to minimize errors and uncertainties. The mean results for each liquid are displayed in Table 4.2.

Table 4.2: *Measured contact angles for the modified liquids with corresponding time and volume, base and height of the droplet.*

Liquid	**Time [s]**	**Contact angle [θ]**	**Volume [µl]**	**Base [mm]**	**Height [mm]**
Water	0.50	92.58	5.81	2.74	1.43
Water (mPEG-RB)	0.50	83.80	4.59	2.73	1.22
PEG 3000	0.50	83.86	5.05	2.82	1.27
PEG 35000	0.50	105.16	6.72	2.55	1.67
pH 2	0.50	96.26	6.48	2.75	1.53
pH 9	0.50	79.74	5.08	2.92	1.22
Tween® 20 (<CMC)	0.50	89.00	5.75	2.82	1.38
Tween® 20 (>CMC)	0.50	88.36	6.15	2.90	1.41
Yes 0.1wt%	0.50	77.96	3.89	2.70	1.09
Yes 0.1wt%	5.00	53.08	3.68	3.27	0.79
Yes 0.05wt%	0.50	85.76	3.85	2.52	1.17
Yes 0.05wt%	5.00	69.90	3.77	2.84	0.99
Yes 0.01wt%	0.50	92.94	6.58	2.85	1.50
Yes 0.01wt%	5.00	89.34	5.90	2.84	1.40
Saccharose	0.50	85.10	5.74	2.91	1.33
NaCl	0.50	88.88	6.96	3.01	1.47

When looking at the liquids containing Yes, Table 4.2 displays two time points. The reason for this is that the liquids modified with Yes showed a decrease in the contact angle during the measurement time. The second time point at five seconds was therefore chosen in order to collect data on the spreading and absorption of the liquids. The liquids modified with Yes, showed a decrease in the contact angle during the measurement time. For the concentration containing 0.1wt% Yes the contact angle decreased by approximately 25° which corresponds to a 32% decrease in contact angle. The solution containing 0.05wt% Yes decrease with 18% and the liquid containing 0.01wt% Yes decrease with 4% in the contact angle. This implies that the absorption is the highest for the liquid containing 0.1wt% Yes compared to the other solutions containing Yes. Table 4.2 also displays that for the liquids with 0.1wt% Yes and 0.05wt% Yes the base increases and the height decreases of the droplet, which means that spreading of the liquids occurs as well as absorption of the liquid which is motivated by the decrease in the volume. The liquid containing 0.1wt% Yes spreads more over the surface than the liquid containing 0.05wt% Yes. The basis of this behavior is that the liquids contain Yes which is a mixture of surfactants. When

looking at the liquid containing 0.01wt% Yes there is an insignificant difference in the base as a function of time yet the height decreases of the droplet which indicates that absorption into the paper is the dominant factor and spreading does not occur.

When observing the values in Table 4.2 the water showed a higher contact angle than water(mPEG-RB) which implies that water(mPEG-RB) is less hydrophilic compared to water. Both Rhodamine B and PEG are hydrophilic compounds but since PEG consists of a hydrophobic tail the compound become less hydrophilic and thus cause a decrease in the contact angle. Since the contact angle for water is >90° and because of its hydrophilicity this indicates that the paper straw material is hydrophobic. As explained in Section 3.2.1.4 the remaining modified liquids did not contain Rhodamine B PEG and hence the remaining results will be compared to water. Due to the fact that Rhodamine B PEG decreases the contact angle the results presented in Table 4.2 will be slightly lower in reality.

Table 4.2 displays that only the liquids modified with PEG 35000 and to pH 2 had a higher contact angle than water. As observed in Section 4.2, PEG 35000 showed a higher surface tension than water and that implies that the contact angle should as well be higher, however, according to Section 2.5.2 polymers generally decrease the surface tension and the contact angle. This is true for PEG 3000 since a decreased contact angle compared to water is observed in Table 4.2. Section 2.5.2 also implies that the higher M_w the lower the contact angle which does not correspond with the results in Table 4.2 and the results obtained for PEG 35000 is probably a measurement error. Since the liquid with pH 2 is modified with HCl, which is a strong electrolyte, the surface tension as well as the contact angle should increase which is confirmed by Table 4.2. The reason why pH 2 increases the contact angle is that the liquid contains electrolytes and electrolytes increase the surface tension since they are reduced from the surface causing a negative adsorption [95]. However this explanation also indicates that the contact angle should increase for pH 9, but as seen in Table 4.2, this has not occurred. A possible explanation for this might be that the concentration of electrolytes in the liquid with pH 9 is less than the concentration of electrolytes in the liquid with pH 2 according to Table 3.2. Electrolytes should increase the contact angle as a function of the concentration of electrolytes but since the concentration of electrolytes is low in the solution with pH 9 compared to pH 2 this behavior is not displayed.

For both the liquids containing Tween® 20, the contact angle is lower than the contact angle for water, this is explained by that Tween® 20 is a non-ionic surfactant. Once the Tween® 20 solution meets the paper straw material the surfactant will lower the interfacial tension by orienting itself to obtain the lowest energy possible for the system. In Table 4.2 the liquid Tween® 20 (>CMC) displays a lower contact angle than Tween® 20 (<CMC), which is explained by the fact that Tween® 20 (>CMC) contains a higher concentration of surfactants and therefore the driving force to obtain the lowest energy is higher compared to the concentration below CMC. The liquids containing Yes with concentration 0.1wt% and 0.05wt% also have a lower contact angle than water and can be explained by the same mechanism as for the liquids

containing Tween® 20. However the liquid with 0.01wt% Yes showed a slightly higher contact angle than water which probably is due to a measurement error.

The liquids containing saccharose and NaCl both decreases the contact angle compared to water which is not desirable results according to Section 2.5.4 and Section 2.5.3. Both of the liquids should increase the surface tension and thereby the contact angle, however, the decrease might be explained by the paper material, which is porous and thereby absorption of the liquid into the paper might occur. To illustrate how the experiments looked like, images from one replicate for each of the two extremes PEG 35000 and Yes 0.1wt% are shown in Figure 4.4.

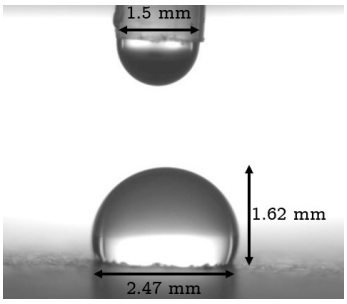

(a) *Contact angle and droplet dimensions for PEG 35000.*

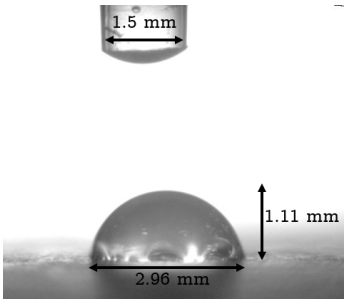

(b) *Contact angle and droplet dimensions for Yes 0.1wt%.*

Figure 4.4: *Images showing one replicate of each extreme from the measured contact angle of the liquids placed upon the paper straw material.*

It can be observed in Figure 4.4 that the dimensions of the droplet differ. PEG 35000 has a shorter base and larger height which means that the liquid spread less over the surface and that the contact angle is larger than the contact angle for Yes 0.1wt%.

4.3 Swelling and penetration of liquids into straw paper

To determine the liquid transport into the straw paper a reference liquid, water(mPEG-RB) was used as explained in Section 3.2.1.3.1. An example of how the CLSM images obtained from the measurement appeared is shown in Figure 4.5. Figure 4.5 displays the cross-section thickness of the paper straw materials autofluorescence as green and the pores inside the cross-section as black. Figure 4.5 also displays the orientation, PS and RS. Figure 4.5 is obtained at time 0s for one of the replicates for water(mPEG-RB) prior to its addition. To further display an example of the obtained results from the CLSM experiments, Figure 4.6 shows the pictures from one time-lapse recording replicate for water(mPEG-RB). The orientation of the cross-section of the paper straw material shown in Figure 4.5 applies to the time-lapse sequence in Figure 4.6.

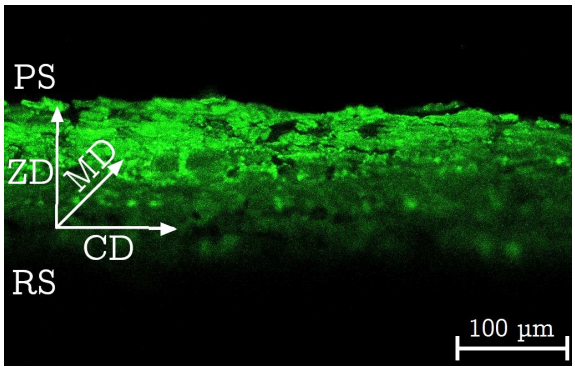

Figure 4.5: *An image captured before addition of water (mPEG-RB) in one CLSM experiment depicts the auto-fluorescence of the paper straw material in green and the pores in black. The cross-section orientation is shown as MD, CD and ZD, along with the two sides PS and RS.*

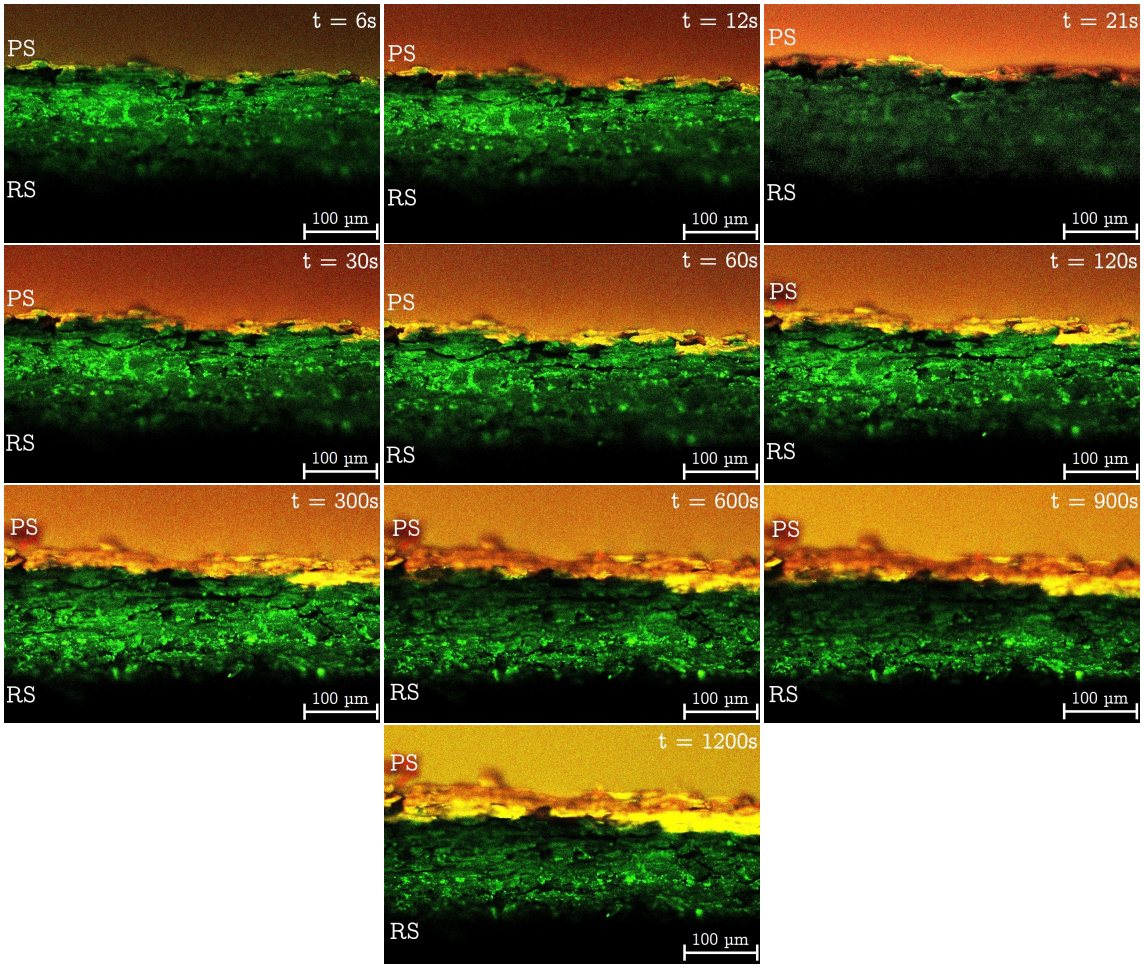

Figure 4.6: *Images from a CLSM time-lapse recording performed with water(mPEG-RB) visualizing the liquid penetration into the cross-section. The cross-section of the paper straw materials auto-fluorescence is shown in green, the pores in black and the water(mPEG-RB) in orange.*

Displayed in Figure 4.6, is the cross-section of the paper straw material in green and the liquid and penetration signal into the cross-section with an orange tone. When observing Figure 4.6 and the specific time points of 6s and 1200s the water(mPEG-RB) distinctly penetrated into the paper straw material. However, when looking at Figure 4.6 and observing the difference between two adjacent time slots the penetration depth can be difficult to behold. Quantitative data from the CLSM measurements were obtained by using image analysis according to Section 3.3. The received data from the image analysis for all CLSM measurements replicates for water(mPEG-RB) is summarized in Figure 4.7.

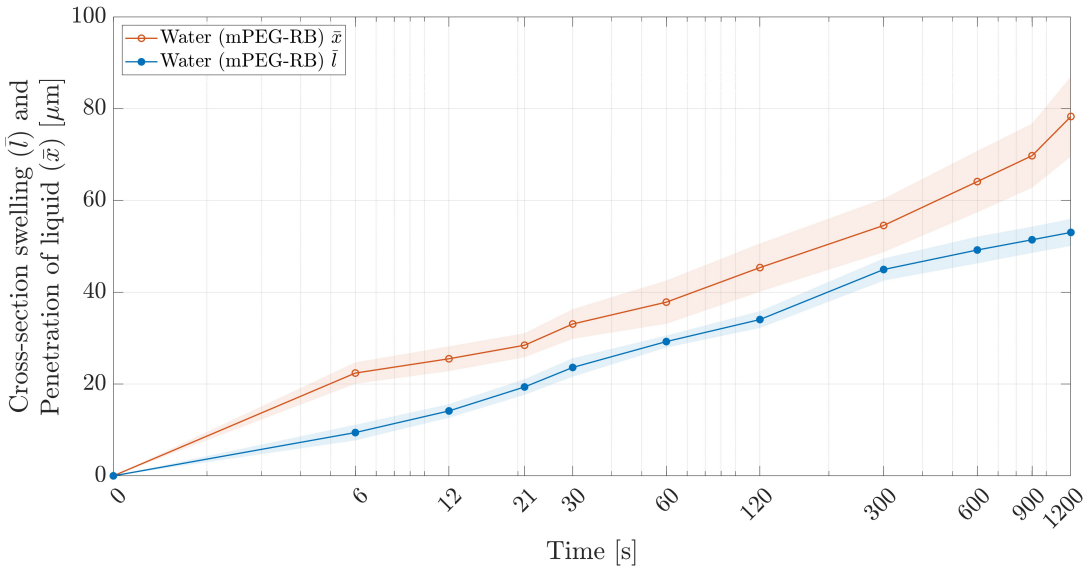

Figure 4.7: *Graph showing the mean cross-section swelling ($\bar{l}$) and the mean penetration depth of liquid ($\bar{x}$) as a function of time from the time-lapse recording replicates of water(mPEG-RB).*

Figure 4.7 displays the cross-section swelling and the penetration depth of the liquid as a function of time in a logarithmic scale on the x-axis. In Figure 4.7 the cross-section swelling is outlined in blue with filled markers and the shaded area next to the line is the standard error for the cross-section swelling, in other words, the variation between the replicates at that specific time point. The liquid penetration depth into the cross-section is shown as the red line with non-filled markers in Figure 4.7 with the standard error displayed as the shaded area next to the line.

As seen in Figure 4.7 the liquid penetrated in total 78 µm into the cross-section thickness which corresponds to 35% and the cross-section swelled 53 µm which corresponds to 33%. The reason why the liquid only penetrated 35% into the cross-section after 1200s could be due to the fact that water(mPEG-RB) is more hydrophilic then the paper straw material and therefore the penetration might be low. When analyzing the penetration depth and the cross-section swelling in Figure 4.7, the lines accompany each other. As a result of the accompanying lines and the fact that Figure 4.6 displays liquid in both the paper fibers and in the pore space the dynamics for water penetration into the paper straw material is considered to follow the mechanisms of liquid transport through paper fibers and capillary transport of liquid through pore space.

4.3.1 Liquid transport as a function of viscosity

This section shows the results of the liquid penetration into the paper straw material and the swelling of the cross-section as a function of viscosity, by the addition of PEG 3000 and PEG 35000. The image analyzed quantitative results from the time-lapse recordings obtained from CLSM are shown in Figure 4.8.

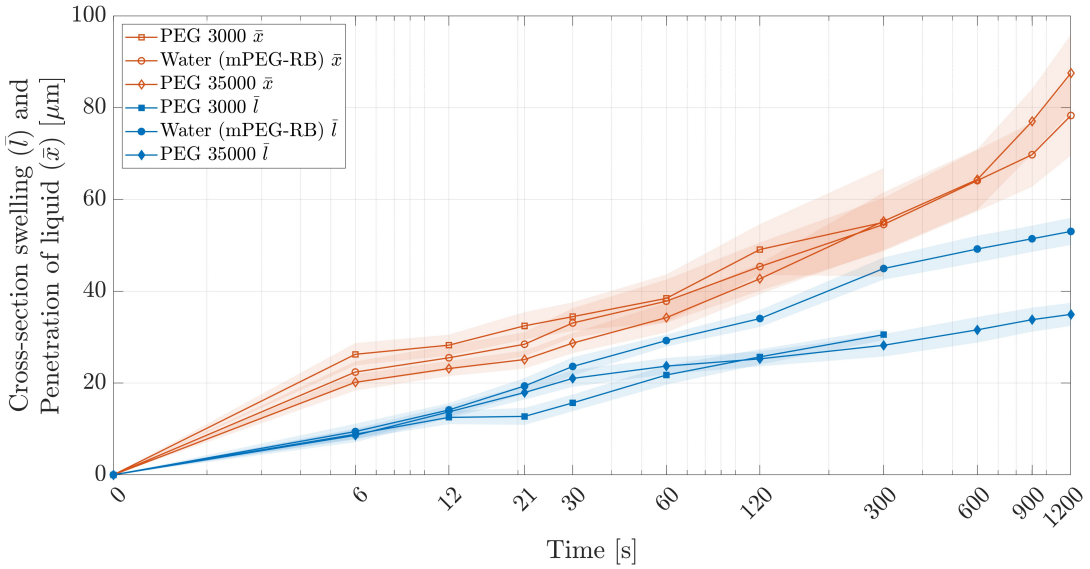

Figure 4.8: *Graph showing the mean cross-section swelling ($\bar{l}$) and the mean penetration depth of liquid ($\bar{x}$) as a function of time from the time-lapse recording replicates of PEG 3000, water(mPEG-RB) and PEG 35 000.*

Figure 4.8 shows the liquid penetration depth into the paper cross-section and the cross-section swelling in µm as a function of time in seconds, displayed in a logarithmic scale on the x-axis. The shaded area around the graphs shows the standard error between replicates of the performed experiments. By observing Figure 4.8 it can be seen that PEG 3000 showed a penetration depth of 49 µm which corresponds to a liquid penetration of 28% into the paper cross-section at 120s. This is deeper than the penetration for water (mPRG-RB) at the same time. PEG 35000 show a penetration depth of 43 µm after 120s, which corresponds to 22% of liquid penetration into the paper cross-section. This is less than the penetration depth for water(mPEG-RB) at the same time. At 300s both PEG 3000 and PEG 35000 show an approximately similar penetration depth as water (mPEG-RB). At 1200s PEG 35000 show a penetration depth of 88 µm which corresponds to 43% of liquid penetration into the cross-section, which is deeper than the penetration for water(mPEG-RB). It can be observed in Figure 4.8 that the swelling of the cross-section is 31 µm which corresponds to 17% of liquid penetration into the cross-section for PEG 3000 and 35 µm which corresponds to 21% of liquid penetration into the cross-section for PEG 35000. Both PEG 3000 and PEG 35000, therefore, show less cross-section swelling than water (mPEG-RB) at 1200s.

Since the liquid penetration of PEG 35000 is slower than water (mPEG-RB) initially, an increased viscosity can have an effect on the liquid penetration rate. However,

PEG 3000, which indeed has a higher viscosity than water (mPEG-RB), shows a faster liquid penetration rate into the material. Thus, the effect of viscosity on liquid penetration rate is not significant and other factors are more dominant in the determination of liquid penetration depth. According to the results in Table 4.1 and Table 4.2 PEG 3000 and PEG 35000 show a lower respectively higher surface tension and contact angle than water (mPEG-RB), which explains why the liquid penetration line for PEG 3000 is located above the line for water (mPEG-RB) and why PEG 35000 is located below water (mPEG-RB). It can from this be concluded that the surface tension and the contact angle have a greater influence on the liquid-paper interaction than the change of the liquid viscosity.

The appearance of the lines showing liquid penetration into the cross-section in Figure 4.8 and the lines showing the cross-section swelling accompany each other well between 12s and 300s. This indicates that the liquid is transported through paper fibers, since the fibers swell when they absorb liquid [38]. It has been shown previously that cellulose chains can form a strong affinity for PEG since they have the possibility to interact through hydrogen bonding [96]. This can be one reason why PEG 3000 and PEG 35000 show liquid transport through paper fibers. Between 0s and 12s as well as after 300s it can be seen that the liquid penetration depth increases faster than the swelling of the paper cross-section. This instead indicates that the liquid is transported through the pores in the paper since the liquid fills up the pores without changing the cross-section thickness of the paper. One explanation for why capillary transport of liquid through pore space also occurs can be that PEG 3000 and PEG 35000 are relatively large molecules and the molecular size can possibly affect the transport mechanism since large molecules probably move easier through the pores than inside the fibers. It can thus be concluded that a combination of liquid transport mechanisms occurs for PEG 3000 and PEG 35000.

As seen in Figure 4.8 the measurements for the liquid modified with PEG 3000 only continue to 300s. The reason for this is that the liquid penetration does not show any clear front and it was therefore impossible to determine the liquid penetration depth after 300s. Figure 4.9 show three selected images captured at different times from one CLSM experiment performed with the PEG 3000.

The images in the first row in Figure 4.9 show the signals obtained from the fiber auto-fluorescence in green, and the fluorescent colourant Rhodamine B PEG in orange, combined in the images. Images in the second row show the signals obtained only from Rhodamine B PEG. When looking at Figure 4.9, it can be observed that the liquid front can be clearly distinguishable after 201s, but at 426s and 816s no clear liquid front can be seen and it is impossible to determine a liquid penetration depth after 300s since the liquid started to flow from different directions after that time. Therefore, the data obtained from the CLSM experiments done with PEG 3000 stops at 300s in Figure 4.8. During measurements of the replicates for PEG 3000, the same behaviour was observed.

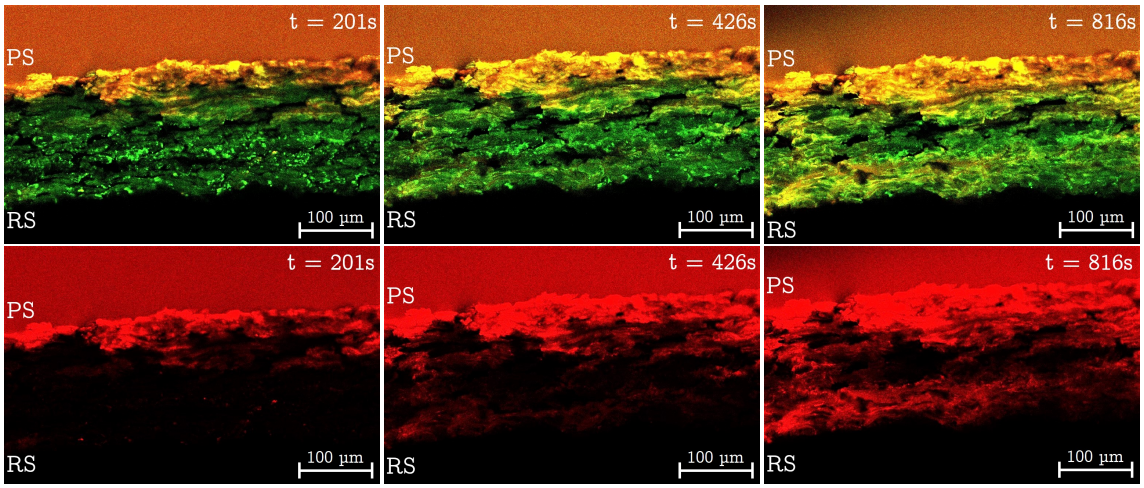

Figure 4.9: *Images from a time-lapse recording obtained from one CLSM experiment performed with PEG 3000 visualizing the penetration of liquid through the cross-section as a function of time. Images in the first row show signals obtained from the fiber auto-fluorescence in green combined with signals obtained from the liquid containing the fluorescent colourant Rhodamine B PEG in orange. The second row show images with signals obtained only from Rhodamine B PEG.*

4.3.2 The effect of pH on liquid transport

In this section the results of how the liquid penetration into the paper straw material and the swelling of the cross-section is affected as a function of pH are displayed. The image analyzed quantitative results from the time-lapse recordings obtained from CLSM are shown in Figure 4.10.

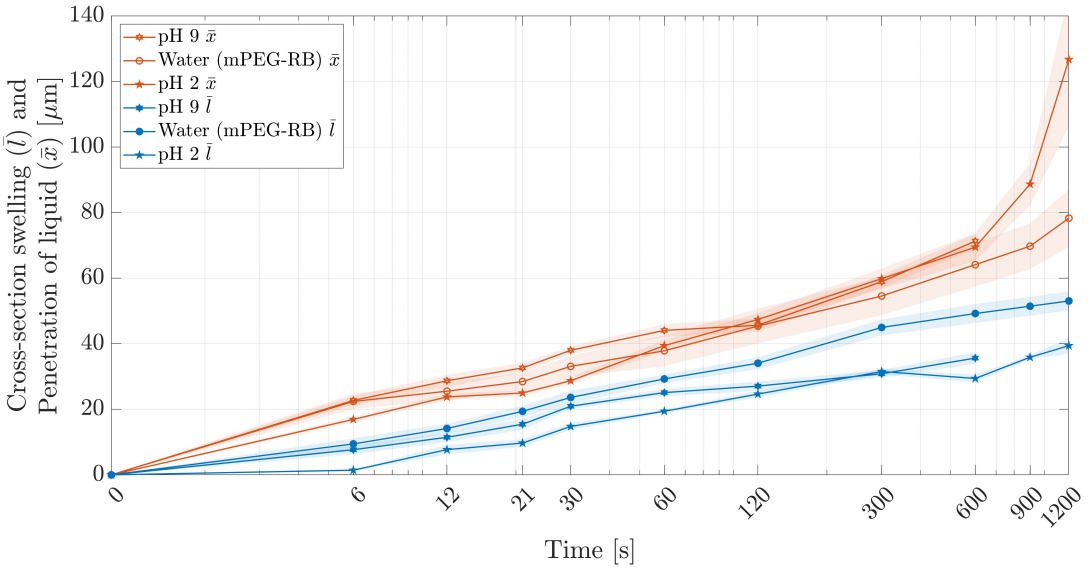

Figure 4.10: *Graph showing the mean cross-section swelling ($\bar{l}$) and the mean penetration depth of liquid ($\bar{x}$) as a function of time from the time-lapse recording replicates of pH 9, water(mPEG-RB) and pH 2.*

Figure 4.10 shows the liquid penetration depth into the paper cross-section and the cross-section swelling in μm as a function of time in seconds, displayed in a logarithmic scale on the x-axis. The shaded area around the graphs shows the standard error between replicates of the performed experiments. During the total measurement time of 1200s, the liquid with a pH of 2 penetrated 127 μm into the cross-section corresponding to 64% while the cross-section swelling was 40 μm corresponding to 25%. According to the results of the water(mPEG-RB) the pH 2 liquid penetrated deeper into the cross-section during the same time. In Figure 4.10, it can be seen that the pH 2 liquid penetrated less deep into the cross-section material compared to water(mPEG-RB) until 30s, however after 60s and until 1200s the penetration rate of pH 2 increased and was higher than the penetration of water(mPEG-RB) into the cross-section thickness.

When observing the liquid with pH 9 in Figure 4.10, the total penetration depth was 71 μm corresponding to 37% while the cross-section swelling was 37 μm corresponding to 23%. The penetration depth of pH 9 was higher than water(mPEG-RB) throughout the measurement time. At 600s both of the liquids with modified pH had penetrated further into the cross-section compared to water(mPEG-RB). This implies that the effect of a pH change of the water(mPEG-RB) resulted in a faster migration of the liquid into the paper, it especially increased the penetration rate after 600s at low pH. However, Figure 4.10 visualize that the cross-section swelling of the paper was lower throughout the measurement time with pH 2 and pH 9 compared to water(mPEG-RB). Since both of the liquids with modified pH gives rise to a smaller amount of swelling the liquid is considered to move more in the pore space and therefore not affect the swelling to an equal extent. When observing the pH 2 lines in the graph between 600s and 1200s the swelling gradient is less than the penetration gradient and therefore the liquid is assumed to move more in the pore space in this interval. Overall the cross-section swelling and the penetration depth of the liquid comply with each other and specific time intervals needs to be observed in order to determine the transport mechanism occurring.

The graph lines in Figure 4.10 indicate that the penetration depth and the cross-section swelling for the pH-modified liquids accompany each other, however, differences can be seen between water(mPEG-RB), pH 2 and pH 9. Since the swelling behavior of the paper straw material is dependent on both the counterion valency, electrolyte concentration and the pH this might be a possible explanation for the difference in the swelling between the pH-modified liquids and water(mPEG-RB) [66]. The difference in observed behavior for pH 2 and pH 9 is independent of the counterion valency and the possible cause is the electrolyte concentration or the pH. A possible reason why the penetration depth of the pH 2 is higher than water(mPEG-RB) might be that the paper straw material, which consists of cellulose, has a higher solubility in extreme pH values [97].

As seen in Figure 4.10 the measurements for pH 9 continued until 600s, due to the non-visible liquid penetration front after 600s. During measurements of the replicates, the same behavior was observed which can be seen in Figure 4.11.

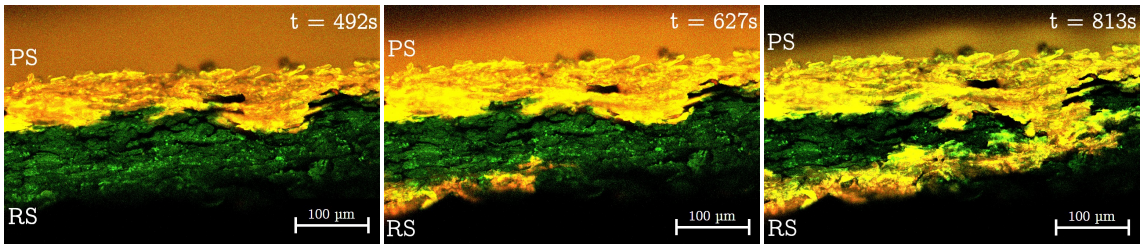

Figure 4.11: *Images from a time-lapse recording obtained from one CLSM experiment performed with pH 9 visualizing the liquid penetration into the cross-section as a function of time. The cross-section's auto-fluorescence is shown in green, the pores in black and the liquid containing the fluorescent colourant Rhodamine B PEG in orange.*

Figure 4.11 displays an example of how the liquid penetration distinguishes from the three transport mechanisms stated in Section 2.3. Figure 4.11 show that pH 9 does not follow the desired path from PS to RS and seems to be more affected by the paper straw material's porosity and orientation. This indicates a faster liquid transport in CD, due to the anisotropy in the straw paper. A possible explanation for the behavior is that the liquid might have penetrated across the cross-section in a non-visible area and then transferred in CD. CD should have more oriented paper fibers than ZD and therefore the dynamics in CD could be more favorable. The observed behavior indicates that the dominant transport mechanisms are liquid transport through paper fibers and capillary transport of liquid through pore space for pH 9.

4.3.3 The influence of emulsifier on liquid transport

The results of how the liquid penetration into the paper straw material and the swelling of the cross-section is affected as a function of emulsifier are shown in this section. The image analyzed quantitative results from the time-lapse recordings obtained from CLSM is shown in Figure 4.12.

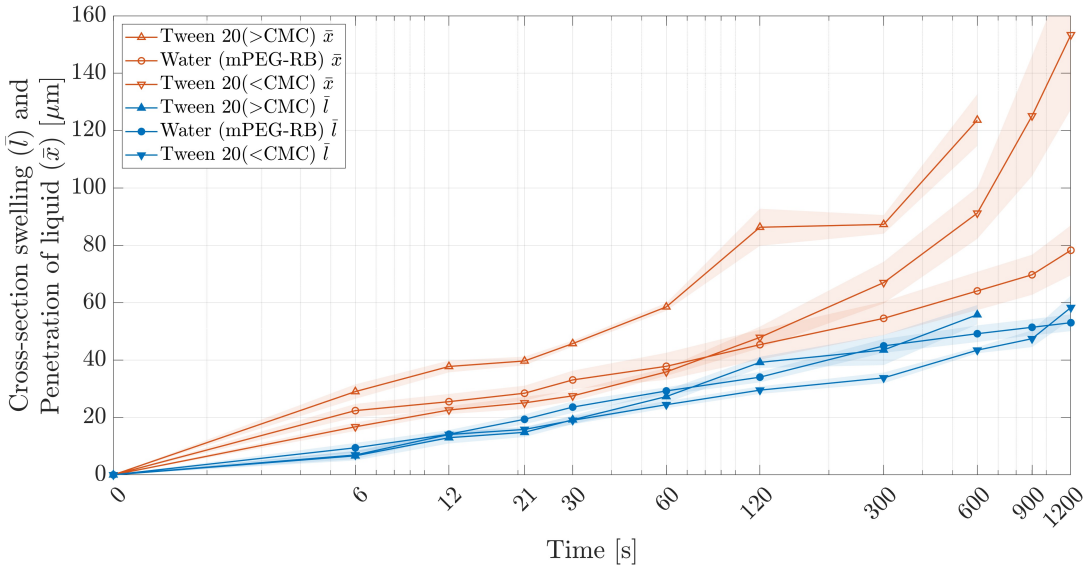

Figure 4.12: *Graph showing the mean cross-section swelling ($\bar{l}$) and the mean penetration depth of liquid ($\bar{x}$) as a function of time from the time-lapse recording replicates of Tween® 20 (>CMC), water(mPEG-RB) and Tween® 20 (<CMC).*

Figure 4.12 shows the liquid penetration depth into the paper cross-section and the cross-section swelling in µm as a function of time in seconds, displayed in a logarithmic scale on the x-axis. The shaded area around the graphs shows the standard error between replicates of the performed experiments. The solution of Tween® 20 (>CMC) penetrated 124µm into the cross-section corresponding to 58% and the cross-section swelling was 56 µm corresponding to 36%. According to the results of the water(mPEG-RB), Tween® 20 (>CMC) penetrated deeper into the cross-section throughout the measurement. Until 60s, the solution containing a concentration below CMC had a penetration depth in µm below the penetration depth of water(mPEG-RB). However, after 120s, the penetration depth of Tween® 20 (<CMC) exceeded the penetration depth of water(mPEG-RB). Tween® 20 (<CMC) penetrated 153 µm corresponding to 74% and the cross-section swelling was 58 µm corresponding to 39% after the total measurement time of 1200s.

The cross-section swelling for both of the solutions containing Tween® 20 showed approximately the same behavior as the water which is shown in Figure 4.12. After 60s both of the solutions containing Tween® 20 exceeded the penetration depth of water(mPEG-RB), this behavior is explained by that the solutions contain surfactants. As proven in Section 4.2, the surface tension of the liquids containing Tween® 20 is decreased compared to water, this affects the liquid penetration. Surfactants always want to minimize the free energy of the system and therefore they orient themselves to the interface which means that the liquid penetrates through the pore space and thereby penetrates faster into the cross-section, however since cross-swelling is observed liquid transport through paper fibers could not be excluded. The reason why the solution containing Tween® 20 above and below CMC differ from each other is due to the concentration inequality, Tween® 20 (>CMC) contains a higher concentration of Tween® 20 and therefore the driving force is larger than for Tween® 20 (<CMC).
As seen in Figure 4.12 the measurement points stop at 600s for Tween® 20 (>CMC), this is due to the behavior observed in Figure 4.13. The behavior made it impossible to determine a clear front of the liquid and thereby the penetration of the liquid could not be evaluated after 600s.

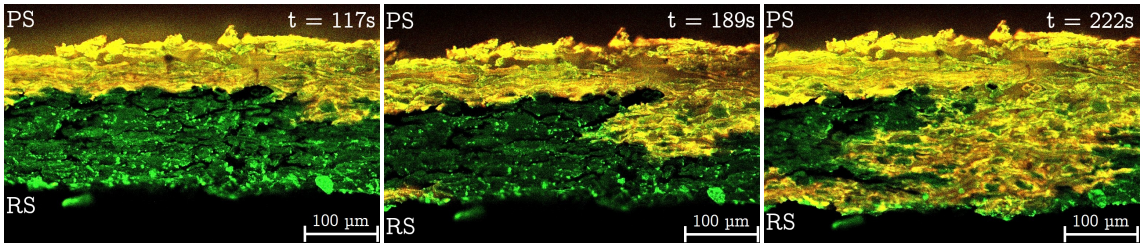

Figure 4.13: *Images from a time-lapse recording obtained from one CLSM experiment performed with Tween® 20 (>CMC) visualizing the penetration of liquid through the cross-section as a function of time. The cross-section of the paper straw materials autofluorescence is shown in green, the pores in black and the liquid containing the fluorescent colourant Rhodamine B PEG in orange.*

The behavior visualized in Figure 4.13 might depend on that the liquid has penetrated throughout the cross-section in a non-visible area and then traveled along the more

aligned CD. The behavior is also similar to the pH 9 modified liquid shown in Figure 4.11 and thus the same possible explanation might also apply in this case.

4.3.4 Liquid transport as a function of surfactant

This section displays the results of the liquid penetration into the paper straw material and the swelling of the cross-section as a function of surfactant. The image analyzed quantitative results from the time-lapse recordings obtained from CLSM is shown in Figure 4.14.

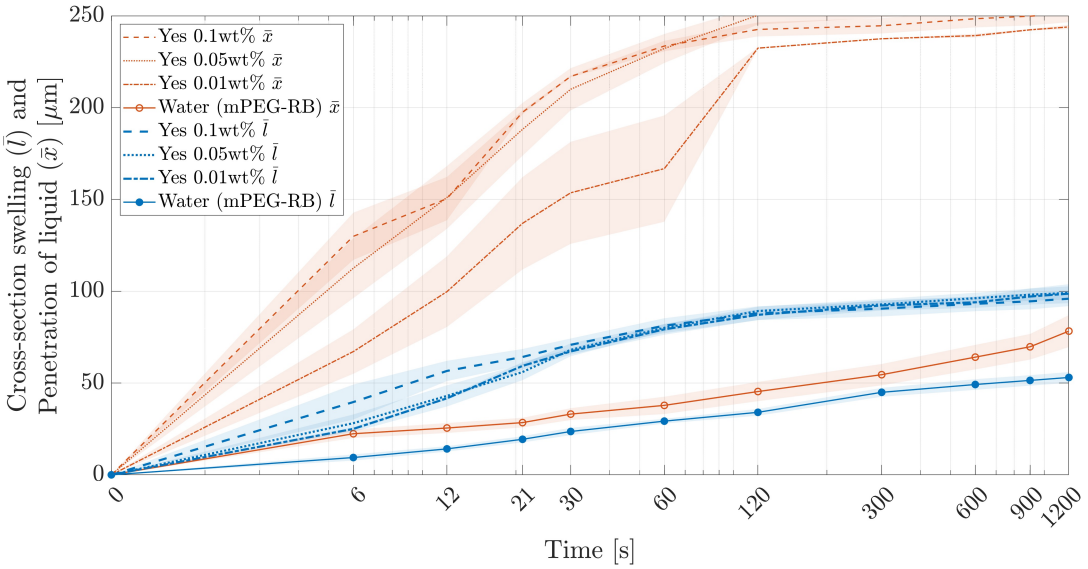

Figure 4.14: *Graph showing the mean cross-section swelling ($\bar{l}$) and the mean penetration depth of liquid ($\bar{x}$) as a function of time from the time-lapse recording replicates of Yes 0.1wt%, Yes 0.05wt%, Yes 0.01 wt% and water(mPEG-RB).*

Figure 4.14 shows the liquid penetration depth into the paper cross-section and the cross-section swelling in µm as a function of time, in a logarithmic scale on the x-axis. During the total measurement time of 1200s, all liquids containing Yes penetrated deeper and at a higher rate into the cross-section of the paper straw material compared to the penetration depth of water (mPEG-RB) after the same time, As seen in Figure 4.14. The penetration depth of liquids containing Yes into the paper cross-section was significant between 0s and 120s, compared to the time span between 120s and 1200s. The reason for this is that the liquids penetrated 100% through the cross-section at 120s, and could not penetrate deeper into the cross-section. In addition, the swelling of the cross-section thickness was larger for all liquids containing Yes than for water (mPEG-RB). The total cross-section swelling after 1200s was 96 µm which correspond to a swelling of 62% for Yes 0.1wt%, 99 µm which corresponds to a swelling of 61% for Yes 0.05wt% and 99 µm which corresponds to a swelling of 68% for Yes 0.01wt%, shown in Figure 4.14.

As seen in Figure 4.14 the standard error is more significant for the liquids containing Yes, both for the liquid penetration and the cross-section swelling, compared to

the standard error for water (mPEG-RB). This means there are more variations between replicates for Yes compared to replicates for water (mPEG-RB). It can also be observed in Figure 4.14 that the difference between the lines showing the liquid penetration and the cross-section swelling is distinctively larger for the liquids containing surfactant, compared to the difference between the lines illustrating water (mPEG-RB) in the graph.

The significantly increased penetration rate of liquids containing Yes compared to water (mPEG-RB) clearly indicates that the effect of adding Yes affects the penetration rate into the cross-section of the paper. Figure 4.14 also show that the lines corresponding to the liquid and cross-section of water are following close to each other, while the gap between the liquid lines and the cross-section lines for Yes is significantly larger. Deeper liquid penetration in relation to the swelling of the cross-section indicates that the liquid transport is dominated by capillary transport through the pore space in the paper since pores filled with liquid should not affect the swelling of the cross-section as much as if the fibers are filled with liquid. However, Figure 4.14 shows that cross-section swelling does occur, which means that the fiber transport mechanism not can be totally excluded. It can also be seen that the concentration of Yes affect both the liquid penetration rate and the cross-section swelling initially. Higher concentration of Yes cause deeper liquid penetration with respect to time, while the opposite can be observed for the swelling of the cross-section, where lower concentrations show more swelling initially.

Yes 0.1wt% and Yes 0.05wt% lower the surface tension of the liquid, as well as the contact angle which is presented in Table 4.1 and 4.2. This appears to favour liquid transport through the pore space in the paper, but also a faster liquid transport. A decreased surface tension and contact angle imply better liquid wetting and spreading over the paper straw material. This makes the liquid flow along the surfaces of the fibers through the cross-section of the paper, which causes the pores to be filled. Yes contains both anionic and zwitterionic surfactants, cellulose has a slight negative charge and like charges repels each other [98]. If the liquid with Yes and the cellulose repel each other this can be one additional reason why the liquid is mainly transported through the pore space and less inside the fibers. However, there are single water molecules present, even though the solutions contain Yes, which can cause the fiber swelling behavior that can be observed in Figure 4.14.

4.3.5 The effect of NaCl or Saccharose on liquid transport

This section displays the results of the liquid penetration into the paper straw material and the swelling of the cross-section as a function of NaCl and saccharose. The image analyzed quantitative results from the time-lapse recordings obtained from CLSM is shown in Figure 4.15.

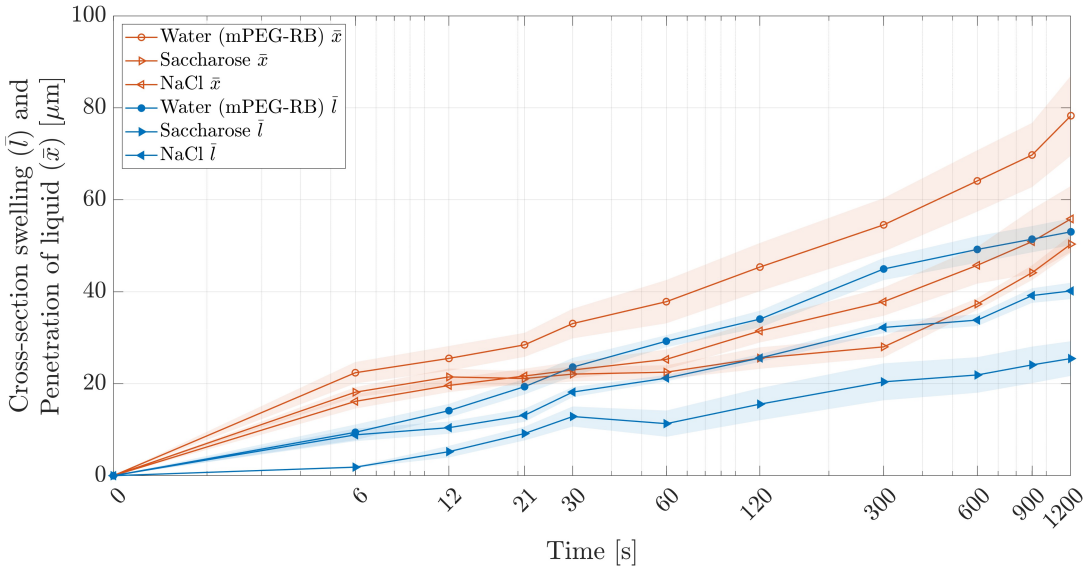

Figure 4.15: *Graph showing the mean cross-section swelling ($\bar{l}$) and the mean penetration depth of liquid ($\bar{x}$) as a function of time from the time-lapse recording replicates of water(mPEG-RB), saccharose and NaCl.*

Figure 4.15 shows the liquid penetration depth into the paper cross-section and the cross-section swelling in µm as a function of time in seconds, displayed in a logarithmic scale on the x-axis. The shaded area around the graphs shows the standard error between replicates of the performed experiments. The solution containing saccharose penetrated 50 µm into the cross-section corresponding to 26% while the cross-section swelling was 25 µm corresponding to 15% until 1200s. The solution with NaCl penetrated 56 µm into the cross-section and the cross-section swelling was 40 µm corresponding to 25% after the measurement time of 1200s. As observed from Figure 4.15, the liquids containing saccharose and NaCl had a cross-section swelling and a penetration depth below water during the entire measurement time.

As mentioned in Section 2.5.3, NaCl is an electrolyte and should therefore increase the surface tension which could lead to a decreased penetration depth. The same argument applies for the saccharose which also should increase the surface tension as mentioned in Section 2.5.3. However, when observing the values in Table 4.1 and Table 4.2 only NaCl showed a slightly higher surface tension compared to water. For the saccharose solution, a possible explanation to why the liquid penetrated a shorter distance could be that the saccharose molecules are bulky and are unable to penetrate through both the paper fiber and the pore space. Between 120s and 300s, Figure 4.15 displays that for the saccharose solution, the cross-section swelling has a higher gradient than the penetration depth which means that vapor diffusion through pore space occurs. From 300s to 1200s the gradient of the penetration depth increases which might be an influence of the vapor diffusion occurring until 300s, due to this the fiber structure becomes more relaxed and the saccharose molecules are thereby able to transport further down in the cross-section. It can also be observed from Figure 4.15 that the cross-section swelling in µm is less than the penetration depth during the total measurement time.

4.3.6 Summary of penetration of liquids into cross-section

In order to summarize the migration studies the penetration depth into the cross-section in % as a function of time is shown in Figure 4.16.

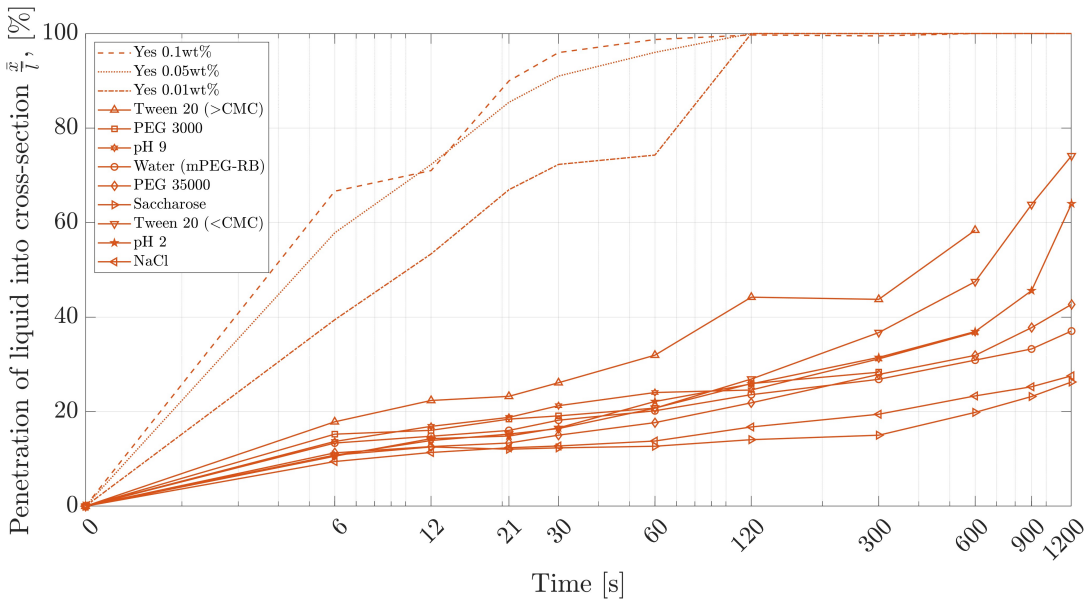

Figure 4.16: *Graph showing the mean penetration depth of all liquids into the cross-section ($\frac{\bar{x}}{l}$) in % as a function of time from the time-lapse recording experiments.*

Figure 4.16 visualizes all evaluated liquids penetration depth into the cross-section as a function of time and it can be seen that all liquids except the ones containing Yes behave similarly to water. Figure 4.16 shows that the liquid penetration exhibits a linear correlation with time for all liquids until 60s. To further evaluate the effect on liquid penetration, a linear approximation was performed for all liquids until 60s. An evaluation of the linear regression coefficient, k, was conducted to determine whether a significant relationship existed according to the liquid properties evaluated, this is shown in Figure 4.17.

Graph (b) in Figure 4.17 visualizes that the pH of the solution do not show a significant correlation to the linear regression coefficient (rate). However, when observing the extremes of pH 2 and pH 9 the rate increases with increasing pH. In graph (b) in Figure 4.17 it is also shown that the liquids with pH between 5-7 all have different initial penetration rate even though the pH difference is not so significant, therefore the pH is not the dominant mechanism for the penetration rate.

From graph (c) in Figure 4.17 it can be observed that the initial penetration rate is independent of the viscosity of the solution, all modified liquids have approximately the same viscosity except for PEG 35000 and graph (c) in Figure 4.17 shows this since PEG 35000 which have a high viscosity do not increase the initial penetration rate. As seen in Figure 4.17, the liquids containing Yes are not included and this is due to the size of the linear regression coefficient, however, the linear regression coefficient for the liquids containing Yes is shown in Figure 4.18.

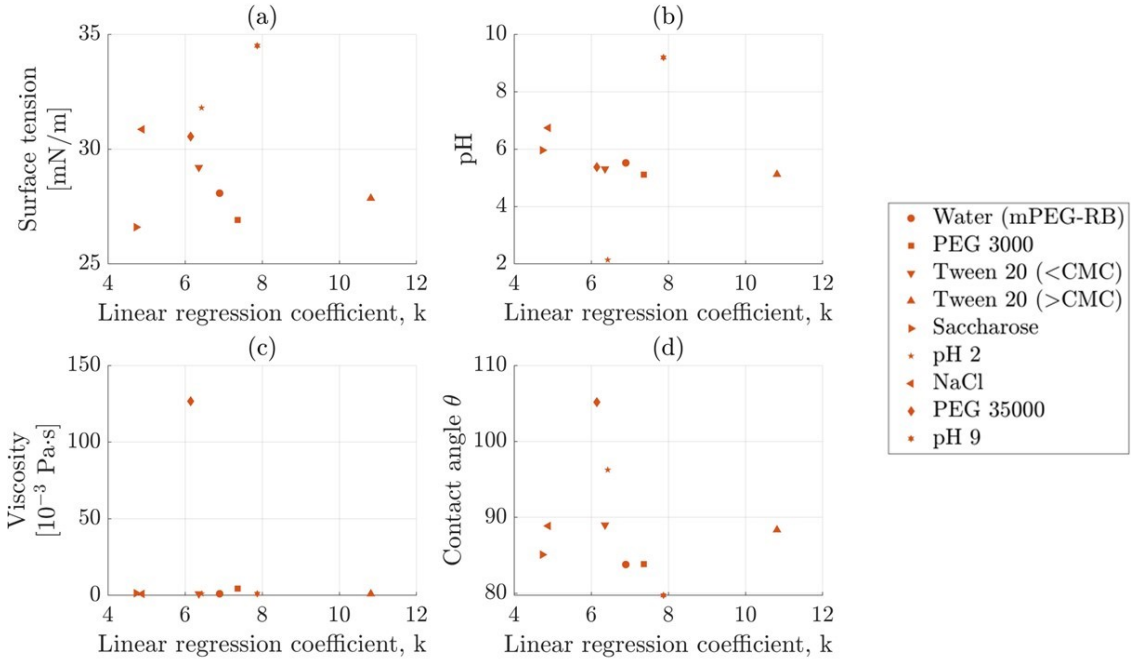

Figure 4.17: *Subplot of graphs showing; (a) surface tension, (b) pH, (c) viscosity and (d) contact angle as a function of the linear regression coefficient k for water(mPEG-RB), PEG 3000, Tween 20, saccharose, pH 2, NaCl, PEG 35000 and pH 9.*

As seen in graph (d) in Figure 4.17 the points are distributed across space, however when excluding NaCl, saccharose and Tween® 20 (>CMC) the penetration rate appears to increase as a function of decreasing contact angle. NaCl and saccharose can be excluded since both of the liquids contain electrolytes which in reality should increase the contact angle and the observed contact angle is probably due to measurement errors. Tween® 20 (>CMC) can be irregular from the trend due to surfactants interacting at the surface. The same behavior observed in graph (d) in Figure 4.17 can be observed graph (a) in Figure 4.17, the initial penetration rate increases with decreasing surface tension.

Figure 4.18 shows that the linear regression coefficient for the liquids containing Yes is higher compared to all the other liquids seen in Figure 4.17. Graph (a) in Figure 4.18 shows the same behavior observed for graph (a) in Figure 4.17, thus that with decreasing surface tension the initial liquid penetration rate increases. The same argument holds for graph (d) in Figure 4.18, with decreasing contact angle the liquid penetration rate increases. Both graph (a) and (d) also show the concentration dependence between the Yes solutions. Graph (b) and (c) in Figure 4.18 visualizes that both the pH and the viscosity have a minor influence on the liquid penetration rate.

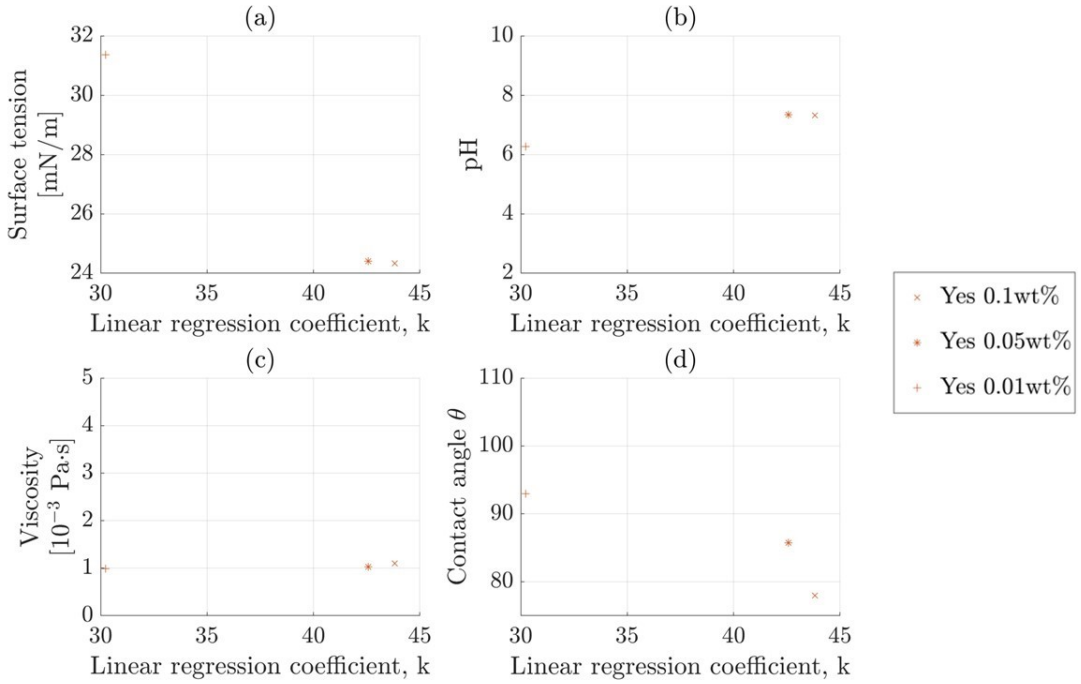

Figure 4.18: *Subplot of graphs showing; (a) surface tension, (b) pH, (c) viscosity and (d) contact angle as a function of the linear regression coefficient k for Yes 0.1wt%, Yes 0.05wt% and Yes 0.01wt%.*

4.4 Liquid transport mechanisms

During the dynamic study of the liquid transport into the straw paper examined by CLSM the three mechanisms explained in Section 2.3 was observed. Water(mPEG-RB) showed a combination of liquid transport through fibers and capillary transport through the pore space. Since all modified liquids are water-based they also show a combination of the transport mechanisms. Examples of the three main mechanisms observed are presented in Figure 4.19.

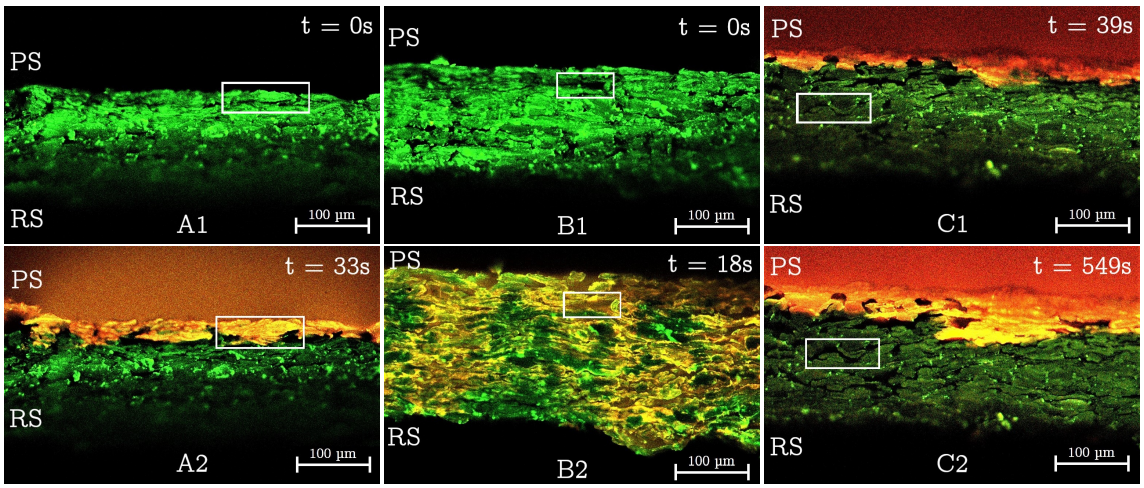

Figure 4.19: *Images of transport mechanisms shown during the CLSM experiments. A1 and A2 show liquid transport through paper fibers. B1 and B2 show capillary transport of liquid through pore space. C1 and C2 show vapor diffusion through pore space.*

A1 and A2 in Figure 4.19, show images from one CLSM experiment where a solution with a pH of 2 was used. A1 shows the cross-section of the paper before the liquid is added, and A2 shows the cross-section of the paper when it has been in contact with the liquid for 33s. The white box highlights an area of the cross-section with a clear fiber region surrounded by a pore space. In A2, it can be seen that the fiber region has been filled with liquid while the surrounding pore space is not filled with liquid. This indicates that the liquid is primarily transported through the fibers, which confirms that the liquid transport in paper fiber displayed in Figure 2.4a occurs. It can also be seen that the fiber area in the white box in A1 swelled when it was filled with liquid in A2. This indicates that the swelling of the cross-section depends on the liquid filling of the fibers.

B1 and B2 in Figure 4.19, show pictures from one CLSM experiment where Yes 0.05wt% was used. B1 shows the cross-section of the paper before the liquid was added, and B2 shows the cross-section of the paper when it has been in contact with the liquid for 18s. The white box highlights an area of the cross-section where a clear pore space can be seen. In B2, it can clearly be seen that this pore is filled with liquid. This indicates that the liquid is primarily transported through the pores, which confirms that the capillary transport through pore space displayed in Figure 2.4b occurs. It can also be seen that the pore space in the white box in B1 remains its size after it has been filled with liquid in B2. This indicates that the liquid filling of the pore space does not affect the swelling of the cross-section as much as if the liquid is transported inside the fibers. B1 and B2 in Figure 4.19 confirm that the main transport mechanism for Yes 0.05wt% is capillary transport in the pore space, which also can be seen for Yes 0.1wt% and 0.01wt% in Figure A.1 in Appendix A. However, it also confirms that some parts of the fiber network are filled with liquid even though the capillary transport through pore space is the dominant mechanism.

C1 and C2 in Figure 4.19, show pictures from one CLSM experiment performed with the NaCl solution. C1 shows the cross-section of the paper after it has been in contact with the liquid for 39s and C2 shows the cross-section of the paper when it has been in contact with the liquid for 549s. The white box highlights an area of the cross-section where a clear pore space is identified. In C2, it can be seen that this pore space has expanded compared to the same pore space in C1, even though the liquid has not reached this area. This indicates that the vapor diffusion mechanism displayed in Figure 2.4c takes place.

5
Conclusion

It was found that the combination of CLSM together with measurement of contact angle, surface tension, viscosity and pH was powerful to investigate the dynamics occurring when liquids with different chemical content and physical properties interact with paper straw material. The results showed a cross-section thickness dependency on RH. Based on the conditioning combined with the ambient climate of the straw material, swelling or shrinking of the cross-section occur as a function of time when the straw paper is exposed to a change in its surrounding conditions. Swelling of the cross-section occurs as a function of increasing RH and shrinking occurs as a function of decreasing RH. The cross-section thickness consequently depends on the storage and surrounding RH and temperature.

The results obtained from the viscosity measurements concluded that PEG 3000 and PEG 35000 showed the most pronounced effect on increasing the viscosity, while the other liquids showed a viscosity similar to water. Measurements of surface tension showed that PEG 35000, NaCl, Yes 0.01wt%, pH 2 and pH 9 increased the surface tension compared to water while PEG 3000, Tween® 20 (<CMC), Tween® 20 (>CMC) Yes 0.1wt%, Yes 0.05wt% and saccharose showed a decreasing effect on surface tension. The liquid characterization also concluded that PEG 3000, PEG 35000, pH 2, Tween® 20 (<CMC) and Tween® 20 (>CMC) showed a lower pH than water while the remaining liquids showed an increased pH. It can also be concluded that the contact angle increased for PEG 35000, pH 2 and Yes 0.01wt% while the other modifiers had a decreasing effect on the contact angle.

From the evaluation of how the properties pH, viscosity and surface tension influence the penetration depth into the paper straw material the following was concluded. The penetration rate did not show a significant dependency on an increased viscosity. The effect of pH change resulted in a faster migration of liquid into the paper straw material and a dependency of the concentration of electrolyte was also significant in this case. It can be concluded that a decrease in surface tension caused an increase in the penetration rate of the liquid into the paper straw material. The increased penetration rate showed dependency on the type of surfactant and its concentration. Surfactants which contains charges on their hydrophilic head group increases the penetration rate to a greater extent compared to surfactants with no charges on the hydrophilic head group. The penetration rate showed a decrease as a function of addition of NaCl or saccharose.

From the evaluation of the cross-section swelling of the paper straw material, it can be concluded that all liquids caused a cross-section swelling as a consequence of liquid penetration into the paper straw material. The cross-section swelling was less for PEG 3000, PEG 35000, pH 2, pH 9, NaCl and saccharose than the cross-section swelling observed for water(mPRG-RB). Tween® 20 (>CMC), Tween® 20 (<CMC) and the liquids containing Yes showed a larger swelling of the cross-section than water(mPRG-RB). The most dominant effect of cross-swelling was observed for the liquids containing Yes, which showed a significantly higher cross-section swelling compared to water(mPRG-RB).

It was concluded that the three transport mechanisms; a) transport through paper fibers, b) capillary transport of liquid through pore space and c) vapor diffusion through pore space all occur. The dominating mechanism occurring for each liquid could not be concluded except for the liquids containing Yes where the dominating mechanism was capillary transport of liquid through pore space. It can however be concluded that the transport mechanism is strongly dependent on the heterogeneity and porosity of the material.

5.1 Proposal for future work

Since the project concludes that pH, surface tension and liquids containing NaCl or saccharose showed an influence on the penetration of liquid into paper straw material further investigations on the influence of these properties could be performed with an increased measurement time.

The project also concluded that the transport mechanisms are strongly dependent on the heterogeneity and the porosity of the paper straw material, in order to determine the dominating transport mechanism and thereby gain extended knowledge about this topic further investigations with other techniques are of interest, for example, X-ray tomography [99]. The project only evaluated the penetration from PS to RS in the ZD of the paper and in order to further give an overview of the liquid transport in straw paper the same procedures should be evaluated in MD and CD as well as from RS. This could also give further information about if the liquid penetration into the paper straw material is affected by the orientation of the paper.

From the in-situ experiments performed in this project, the gained information could also be used in possible modeling techniques in order to visualize the results as well as to confirm the outcome shown in the project.

Bibliography

[1] Körber AG . Hauni Straw Maker [Internet]. Hamburg: Körber AG; 2023 [cited 2023 Mar 28]. Available from: https://www.koerber-technologies.com/fileadmin/Media/Images/Food-Beverages/OnePager_HSM_MM.pdf.

[2] Lorén N, Langton M, Hermansson AM. 9 - Confocal fluorescence microscopy (CLSM) for food structure characterisation. In: McClements DJ, editor. Understanding and Controlling the Microstructure of Complex Foods [Internet]. Sawston, Cambridge, England: Woodhead Publishing; 2007 [cited 2023 Jan 18]. p.232–60. DOI: 10.1533/9781845693671.2.232.

[3] Our World in Data. Population, 10,000 BCE to 2021 [Internet]; 2021 [cited 2023 Mar 4]. Available from: https://ourworldindata.org/grapher/population.

[4] Dong T, Chen W, Cai C, Bai F, Zhou Z, Wang J, et al. Water-stable, strong, biodegradable lignocellulose straws replacement for plastic straws. Chem Eng J Ad [Internet]. 2023 [cited 2023 Jan 17];451(4):138970. DOI: 10.1016/j.cej.2022.138970.

[5] Sin LT, Tueen BS. 1 - Plastics and environmental sustainability issues. In: Lee TS and Tueen BS, editors. Plastics and Sustainability [Internet]. Amsterdam, Elsevier; 2023 [cited 2023 Mar 16] p. 1-43. DOI: 10.1016/B978-0-12-824489-0.00006-4.

[6] European Commission. EU restrictions on certain single-use plastics [Internet]. Strasbourg: European Commission; [date unknown; cited 2023 Jan 18]. Available from: https://environment.ec.europa.eu/topics/plastics/single-use-plastics/eu-restrictions-certain-single-use-plastics_en.

[7] Tetra Pak®. Tetra Pak becomes first carton packaging company to launch paper straws in Europe [Internet]. Lausanne, Switzerland: Tetra Pak®; 2019 [cited 2023 Jan 23]. Available from: https://www.tetrapak.com/about-tetra-pak/news-and-events/newsarchive/first-carton-packaging-company-to-launch-paper-straws.

[8] Zhou X, Yi C, Deng D. Sustainable development strategy of beverage straws for environmental load reduction. IOP Conf Ser Earth Environ Sci [Internet]. 2021 [cited 2023 Jan 17];784(1):012041. DOI: 10.1088/1755-1315/784/1/012041.

[9] Alexandersson M. Macroscopic modelling of coupled multiphysics in swelling cellulose based materials [Dissertation on the Internet]. Lund, Sweden: Lund University; 2020 [cited 2023 Jan 23]. Available from: https://lup.lub.lu.se/search/files/83092731/Marcus_Alexandersson_web.pdf.

[10] Öhgren C. In situ vätning av sugrörspapp i CLSM [Internal Power Point]. Gothenburg: RISE; 2022 [cited 2023 Feb 8]. Available from: Internal meeting RISE Agriculture and Food.

[11] Andreasson E, Lindström T, Gunsjö H, Jönsson G, Bergvall E, Nordgren J, et al. Paper Straw Development guided by Virtual Modelling - Physical tests in combination with virtual tests (FEM/CFD) [Internet]. 2021 [cited 2023 Feb 2]. Available from: https://www.researchgate.net/publication/355172151_Paper_Straw_Development_guided_by_Virtual_Modelling_-_Physical_tests_in_combination_with_virtual_tests_FEMCFD.

[12] Wang X, Xia Q, Jing S, Li C, Chen Q, Chen B, et al. Strong, Hydrostable, and Degradable Straws Based on Cellulose-Lignin Reinforced Composites. Small [Internet]. 2021 [cited 2023 Mars 23];17(18):p.2008011. DOI: 10.1002/smll.202008011.

[13] Habibi Y, Lucia LA, Rojas OJ. Cellulose Nanocrystals: Chemistry, Self-Assembly, and Applications. Chem Rev [Internet]. 2010 [cited 2023 Mars 23];110(6):p.3479-500. DOI: 10.1021/cr900339w.

[14] Ragnar M, Henriksson G, Lindström ME, Wimby M, Blechschmidt J, Heinemann S. Pulp. In: Ullmann F, editor. Ullmann's Encyclopedia of Industrial Chemistry. [Internet]. Berlin, Germany: John Wiley & Sons, Ltd; 2014 [cited 2023 Mars 23] p.1-92. DOI: 10.1002/14356007.a18_545.pub4.

[15] Fahlén J. The cell wall ultrastructure of wood fibres : effects of the chemical pulp fibre line [Dissertation on the Internet]. Stockholm: KTH Royal Institute of Technology; 2005 [cited 2023 Mars 23]. Available from: https://www.diva-portal.org/smash/get/diva2:7109/FULLTEXT01.pdf.

[16] Goldstein IS. WOOD FORMATION AND PROPERTIES | Chemical Properties of Wood. In: Burley J, editor. Encyclopedia of Forest Sciences. [Internet]. Oxford, UK: Elsevier; 2004 [cited 2023 Feb 13] p.1835-39. DOI: 10.1016/B0-12-145160-7/00042-9.

[17] Auhorn WJ. Chapter 3 - Chemical Additives. In: Holik H, editor. Handbook of Paper and Board [Internet]. Ravensburg, Germany: John Wiley & Sons, Ltd; 2006 [cited 2023 Mar 8]. p. 62-149. DOI: 10.1002/3527608257.ch3.

[18] Holik H, Tschudin PF, Rentrop GH. Chapter 1 - Introduction. In: Holik H, editor. Handbook of Paper and Board [Internet]. Ravensburg, Germany: John Wiley & Sons, Ltd; 2006 [cited 2023 Mars 8]. p. 1-19. DOI: 10.1002/3527608257.ch1.

[19] Blechschmidt J, Heinemann S, Putz HJ, Laufmann M, Kogler W, Gliese T, et al. Chapter 2 - Raw Materials for Paper and Board Manufacture. In: Holik H, editor. Handbook of Paper and Board [Internet]. Ravensburg, Germany: John Wiley & Sons, Ltd; 2006 [cited 2023 Mars 8]. p. 20-61. DOI: 10.1002/3527608257.ch2.

[20] Jern D, Leek A. Sharp Edge Cutting Through Paperboard [Dissertation on the Internet]. Lund: Lund University; 2017 [cited 2023 Feb 22]. Available from: https://lup.lub.lu.se/luur/download?func=downloadFile&recordOId=8917809&fileOId=8917813.

[21] Holik H, Gamsjäger N, Westerkamp A, Schmitt MW, Morton A, Stetter A, et al. Chapter 6 - Paper and Board Manufacturing. In: Holik H, editor. Handbook of Paper and Board [Internet]. Ravensburg, Germany: John Wiley & Sons, Ltd; 2006 [cited 2023 Mars 8]. p. 219-331. DOI: 110.1002/3527608257.ch6.

[22] Tetra Pak®. Paper two-sidedness [Internal Power Point]. Lund: Tetra Pak®; 2020 [cited 2023 Apr 3]. Available from: Internal meeting Tetra Pak®.

[23] Holmen Paper. The third step of paper production: From pulp to paper [Internet]; 2023 [cited 2023 Feb 2]. Available from: https://www.holmen.com/en/paper/insights/paper-academy/paper-production/from-pulp-to-paper/.

[24] Bajpai P. Chapter 2 - Wood and Fiber Fundamentals. In: Biermann's Handbook of Pulp and Paper (Third Edition) [Internet]. Kanpur, India: Elsevier; 2018 [cited 2023 Jan 18]. p. 19-74. DOI: 10.1016/B978-0-12-814240-0.00002-1.

[25] Marin G. Impact of paperboard deformation and damage mechanisms on packaging performance [Licentiate Thesis on the Internet]. Stockholm: KTH Royal Institute of Technology; 2023 [cited 2023 Mar 28]. Available from: http://kth.diva-portal.org/smash/get/diva2:1738574/FULLTEXT01.pdf.

[26] Hobisch MA, Bossu J, Mandlez D, Bardet SM, Spirk S, Eckhart R, et al. Localization of cellulosic fines in paper via fluorescent labeling. Cellulose (Lond) [Internet]. 2019 [cited 2023 Jan 24];26(11):6933-42. DOI: 10.1007/s10570-019-02556-0.

[27] Körber AG . Paper not plastic [Internet]. Hamburg: Körber AG; 2023 [cited 2023 Mar 28]. Available from: https://www.koerber-technologies.com/en/news-stories/paper-not-plastic.

[28] Alexandersson M, Ristinmaa M. Modelling multiphase transport in deformable cellulose based materials exhibiting internal mass exchange and swelling. International Journal of Engineering Science [Internet]. 2018 [cited 2023 Apr 2];128(7):101-26. DOI: 10.1016/j.ijengsci.2018.03.013.

[29] Perkins EL, Batchelor WJ. Water interaction in paper cellulose fibres as investigated by NMR pulsed field gradient. Carbohydr Polym [Internet]. 2012 [cited 2023 Apr 2];87(1):361-7. DOI: 10.1016/j.carbpol.2011.07.065.

[30] Kupczak A, Bratasz L, Krysciak-Czerwenka J, Kozlowski R. Moisture sorption and diffusion in historical cellulose-based materials. Cellulose (Lond) [Internet]. 2018 [cited 2023 Apr 3];25(5):2873-84. DOI: 10.1007/s10570-018-1772-9.

[31] Salminen P. Studies of Water Transport in Paper during Short Contact Times [Internet]. Åbo; 1988 [cited 2023 Apr 3]. Available from: https://www.researchgate.net/profile/Pekka-Salminen/publication/35946579_Studies_of_Water_Transport_in_Paper_during_Short_Contact_Times/links/58be789692851cbe16e034dd/Studies-of-Water-Transport-in-Paper-during-Short-Contact-Times.pdf.

[32] Marin G. On the relation between paperboard properties and packaging performance [Licentiate thesis on the Internet]. Stockholm, Sweden: KTH Royal Institute of Technology; 2021 [cited 2023 May 3]. Available from: http://kth.diva-portal.org/smash/record.jsf?pid=diva2%3A1508084&dswid=-8686.

[33] Małachowska E, Dubowik M, Boruszewski P, Łojewska J, Przybysz PJ. Influence of lignin content in cellulose pulp on paper durability. Scientific Reports [Internet]. 2020 [cited 2023 May 3];10. DOI: 10.1038/s41598-020-77101-2.

[34] RISE Research Institutes of Sweden. The weather fluctuations affect the testing of cellulose products [Internet]. Örnsköldsvik: RISE; (n.d) [cited 2023 Mar 28]. Available from: https://www.ri.se/en/what-we-do/services/the-weather-fluctuations-affect-the-testing-of-cellulose-products.

[35] Thybring EE, Fredriksson M, Zelinka SL, Glass SV. Water in Wood: A Review of Current Understanding and Knowledge Gaps. Forests [Internet]. 2022 [cited 2023 Apr 5];13(12):2051. DOI: 10.3390/f13122051.

[36] Marmur A. Kinetics of Penetration into Uniform Porous Media: Testing the Equivalent-Capillary Concept. Langmuir [Internet]. 2003 [cited 2023 May 16];19(14):5956-9. DOI: 10.1021/la034490v.

[37] Oko A, Claesson P, Swerin A. Imbibition and Evaporation of Water Droplets on Paper and Solid Substrates. Journal of Imaging Science and Technology [Internet]. 2011 [cited 2023 May 17];55(1):10201. Available from: http://urn.kb.se/resolve?urn=urn:nbn:se:kth:diva-31330.

[38] Patari S, Sinha Mahapatra P. Imbibition of Liquids through a Paper Substrate in a Controlled Environment. Langmuir [Internet]. 2022 [cited 2023 May 10];38(15):4736-46. DOI: 10.1021/acs.langmuir.2c00318.

[39] Liu G, Fu S, Zhang M, Wang Y. Analysis and Measurement of the Imbibition Characteristic of Paper Based in the y-Direction. In: Zhao P, Ouyang Y, Xu M, Yang L and Ren Y, editors. Applied Sciences in Graphic Communication and Packaging [Internet]. Singapore: Springer Singapore; 2018 [cited 2023 May 17] p.581-90. DOI: 10.1007/978-981-10-7629-9_71.

[40] Chang S, Kim W. Dynamics of water imbibition through paper with swelling. Flow (Camb) [Internet]. 2020 [cited 2023 May 17];892:A39. DOI: 10.1017/jfm.2020.219.

[41] Zhang G, Parwani R, Stone CA, Barber AH, Botto L. X-ray Imaging of Transplanar Liquid Transport Mechanisms in Single Layer Textiles. Langmuir [Internet]. 2017 [cited 2023 May 17];33(43):12072-9. DOI: 10.1021/acs.langmuir.7b02982.

[42] Bencsik M, Adriaensen H, Brewer SA, McHale G . Quantitative NMR monitoring of liquid ingress into repellent heterogeneous layered fabrics. J Magn Reson [Internet]. 2008 [cited 2023 May 17];193(1):32-6. DOI: 10.1016/j.jmr.2008.04.003.

[43] Birrfelder P, Dorrestijn M, Roth C, Rossi R. Effect of fiber count and knit structure on intra- and inter-yarn transport of liquid water. Text Res J [Internet]. 2013 [cited 2023 May 17];83:1477-88. DOI: 10.1177/0040517512460296.

[44] Canette A, Briandet R. MICROSCOPY | Confocal Laser Scanning Microscopy. In: Batt CA & Tortorello ML, editors. Encyclopedia of Food Microbiology. 2. ed. [Internet]. Oxford, England: Academic Press; 2014 [cited 2023 Jan 18]. p.676–83. DOI: 10.1016/B978-0-12-384730-0.00214-7.

[45] Gratton E, vandeVen MJ. Laser Sources for Confocal Microscopy. In: Pawley JB, editor. Handbook Of Biological Confocal Microscopy [Internet]. Boston, MA: Springer US; 2006 [cited 2023 Jan 18]. p.80–125. DOI: 10.1007/978-0-387-45524-2_5.

[46] PubChem [Internet]. Bethesda (MD): National Library of Medicine (US), National Center for Biotechnology Information; 2004-. Rhodamine B. [cited 2023

Mar 14]. Available from: https://pubchem.ncbi.nlm.nih.gov/compound/Rhodamine-B.

[47] Nanocs Inc. Rhodamine B PEG, MW 1000, 2000, 5000, 10k, 20k, 30k. [Internet]. Boston: Nanocs Inc; 2023 [cited 2023 Jan 23]. Available from: http://www.nanocs.net/document/DataSheet/mPEG-Rhodamine-B-DataSheet-NANOCS.pdf.

[48] Schroeder AB, Dobson ETA, Rueden CT, Tomancak P, Jug F, Eliceiri KW. The ImageJ ecosystem: Open-source software for image visualization, processing, and analysis. Protein Science [Internet]. 2021 [cited 2023 Apr 5];30(1):234-49. DOI: 10.1002/pro.3993.

[49] Alghunaim A, Kirdponpattara S, Newby BZ. Techniques for determining contact angle and wettability of powders. Powder Technology [Internet]. 2016 [cited 2023 Apr 18];287:201-15. DOI: 10.1016/j.powtec.2015.10.002.

[50] Huhtamäki T, Tian X, Korhonen JT. Surface-wetting characterization using contact-angle measurements. Nat Protoc [Internet]. 2018 [cited 2023 Jan 17];13(7):1521-38. DOI: 10.1038/s41596-018-0003-z.

[51] Hansen FK, Rødsrud G. Surface tension by pendant drop: I. A fast standard instrument using computer image analysis. JCIS open [Internet]. 1991 [cited 2023 Apr 18];141(1):1-9. DOI: 10.1016/0021-9797(91)90296-K.

[52] Holmberg K, Lindman B, Kronberg B. Chapter 12. Surface and Interfacial Tension. In: Surface Chemistry of Surfactants and Polymers [Internet]. Boca Raton: John Wiley & Sons; 2014 [cited 2023 Apr 19] p. 231-250. Available from: https://ebookcentral.proquest.com/lib/chalmers/detail.action?docID=1791862.

[53] Kwok DY, Neumann AW. Contact angle measurement and contact angle interpretation. Adv Colloid Interface Sci [Internet]. 1999 [cited 2023 Jan 17];81(3):167-249. DOI: 10.1016/S0001-8686(98)00087-6.

[54] Schulman T. Fundamental concepts of wettability, contact angle and surface tension [Internal Power Point]. Lund: Tetra Pak®; 2020 [cited 2023 Feb 8]. Available from: Internal meeting Tetra Pak®.

[55] Prakash CGJ, Prasanth R. Approaches to design a surface with tunable wettability: a review on surface properties. Journal of Materials Science [Internet]. 2021 [cited 2023 Jan 23];56(1):1-28. DOI: 10.1007/s10853-020-05116-1.

[56] Rosenholm JB. Liquid spreading on solid surfaces and penetration into porous matrices: Coated and uncoated papers. Adv Colloid Interface Sci [Internet]. 2015 [cited 2023 Mar 3];220:8-53. DOI: 10.1016/j.cis.2015.01.009.

[57] Khan Academy. Cohesion and adhesion of water [Internet]. Mountain View: Khan Academy; 2023 [cited 2023 Apr 25]. Available from: https://www.khanacademy.org/science/ap-biology/chemistry-of-life/structure-of-water-and-hydrogen-bonding/a/cohesion-and-adhesion-in-water.

[58] Krainer S, Hirn U. Contact angle measurement on porous substrates: Effect of liquid absorption and drop size. Colloids and Surfaces A: Physicochemical and Engineering Aspects [Internet]. 2021 [cited 2023 Apr 18];619:126503. DOI: 10.1016/j.colsurfa.2021.126503.

[59] Winkler T. Pendant drop measurements [Internet]. Hamburg: Krüss; 2010 [cited 2023 Apr 18]. Available from: https://warwick.ac.uk/fac/cross_fac/sciencecity/programmes/internal/themes/am2/booking/dropshapeanalyser/kruss-tn316-en.pdf.

[60] Berry JD, Neeson MJ, Dagastine RR, Chan DYC, Tabor RF. Measurement of surface and interfacial tension using pendant drop tensiometry. JCIS Open [Internet]. 2015 [cited 2023 Apr 18];454:226-37. DOI: 10.1016/j.jcis.2015.05.012.

[61] Lauren S. Pendant drop method for surface tension measurements [Internet]. Gothenburg: Biolinscientific; 2020 [cited 2023 Apr 18. Available from: https://www.biolinscientific.com/blog/pendant-drop-method-for-surface-tension-measurements.

[62] Webster D. PH – PRINCIPLES AND MEASUREMENT. In: Caballero B, editor. Encyclopedia of Food Sciences and Nutrition (Second Edition) [Internet]. Oxford, England: Academic Press; 2003 [cited 2023 Apr 3]. p.4501-4507. DOI: 10.1016/B0-12-227055-X/00913-5.

[63] Weiner RF, Matthews RA. Chapter 5 - Measurement of Water Quality. In: Ruth F. Weiner and Robin A. Matthews, editors. Environmental Engineering (Fourth Edition) [Internet]. Burlington, U.S: Butterworth-Heinemann; 2003 [cited 2023 Apr 3]. p.81-106. DOI: 10.1016/B978-075067294-8/50005-1.

[64] Bäckström M. The effect of environment on refining efficiency of kraft pulps [Dissertation on the Internet]. Stockholm: KTH Royal Institute of Technology; 2020 [cited 2023 Apr 3]. Available from: http://www.diva-portal.org/smash/get/diva2:1456955/FULLTEXT01.pdf.

[65] Jansson J. The influence of pH on fiber and paper properties [Dissertation on the Internet]. Karlstad: Karlstad University; 2015 [cited 2023 Apr 3]. Available from: https://www.diva-portal.org/smash/get/diva2:823180/FULLTEXT01.pdf.

[66] Österbeg M, Claesson PM. Interactions between cellulose surfaces: effect of solution pH. J Adhes Sci Technol [Internet]. 2000 [cited 2023 Apr 3];14(5):p. 603-18. DOI: 10.1163/156856100742771.

[67] Rehman A, Tong Q, Shehzad Q, Aadil RM, Khan IM, Riaz T, et al. Chapter Sixteen - Rheological analysis of solid-like nanoencapsulated food ingredients by rheometers. In: Jafari SM, editor. Characterization of Nanoencapsulated Food Ingredients [Internet]. Gorgan: Academic Press; 2020 [cited 2023 Mar 20] p. 547-583. DOI: 10.1016/B978-0-12-815667-4.00016-X.

[68] Østergård AL. Different Types of Rheometers [Internet]. Copenhagen: Fluidan; 2021 [cited 2023 Jan 24]. Available from: https://fluidan.com/different-types-of-rheometers/.

[69] Anton Paar GmbH. Rheometer geometries: relative measuring geometries [Internet]. Graz: Anton Paar GmbH; 2023 [cited 2023 Jan 18]. Available from: https://wiki.anton-paar.com/en/rheometer-geometries-relative-measuring-geometries/.

[70] Anton Paar GmbH. How to measure viscosity [Internet]. Graz: Anton Paar GmbH; 2023 [cited 2023 Mar 20]. Available from: https://wiki.anton-paar.com/en/how-to-measure-viscosity/.

[71] Perugini L, Cinelli G, Cofelice M, Ceglie A, Lopez F, Cuomo F. Effect of the coexistence of sodium caseinate and Tween 20 as stabilizers of food emulsions at acidic pH. Colloids Surf B Biointerfaces [Internet]. 2018 [cited 2023 Mar 3];168(8):163-8. DOI: 10.1016/j.colsurfb.2018.02.003.

[72] Holmberg K, Lindman B, Kronberg B. Chapter 1. Types of Surfactants, their Synthesis, and Applications. In: Surface Chemistry of Surfactants and Polymers [Internet]. Boca Raton: John Wiley & Sons, Incorporated; 2014 [cited 2023 Mar 3] p. 1-48. Available from: https://ebookcentral.proquest.com/lib/chalmers/reader.action?docID=1791862.

[73] Holmberg K, Lindman B, Kronberg B. Chapter 8. Surfactant Adsorption at Solid Surfaces. In: Surface Chemistry of Surfactants and Polymers [Internet]. Boca Raton: John Wiley & Sons, Incorporated; 2014 [cited 2023 Mar 3] p. 153-74. Available from: https://ebookcentral.proquest.com/lib/chalmers/reader.action?docID=1791862.

[74] Hempel NJ, Dao T, Knopp MM, Berthelsen R, Löbmann K. The Influence of Temperature and Viscosity of Polyethylene Glycol on the Rate of Microwave-Induced In Situ Amorphization of Celecoxib. Molecules [Internet]. 2020 [cited 2023 Mar 10];26(1):1-9. DOI: 10.3390/molecules26010110.

[75] Aronson JK. Glycols. In: J.K. Aronson, editor. Meyler's Side Effects of Drugs (Sixteenth Edition) [Internet]. Oxford, England: Elsevier; 2016 [cited 2023 Mar 10]. p.567-570. DOI: 10.1016/B978-0-444-53717-1.00816-7.

[76] Sigma-Aldrich, Inc . Polyethylene Glycol (PEG) Selection Guide [Internet]. Darmstadt: Germany; c 2023 [cited 2023 Mar 10]. Available from: https://www.sigmaaldrich.com/SE/en/technical-documents/technical-article/materials-science-and-engineering/drug-delivery/polyethylene-glycol-selection-guide.

[77] Cowie JMG, Valeria A. Chapter 13. Rheology and Mechanical Properties. In: Polymers : Chemistry and Physics of Modern Materials, Third Edition [Internet]. London: Taylor & Francis Group; 2007 [cited 2023 Apr 19] p. 345-88. Available from: https://ebookcentral.proquest.com/lib/chalmers/detail.action?docID=1449424.

[78] Holmberg K, Lindman B, Kronberg B. Chapter 11. Adsorption of Polymers at Solid Surfaces. In: Surface Chemistry of Surfactants and Polymers [Internet]. Boca Raton: John Wiley & Sons, Incorporated; 2014 [cited 2023 Apr 19] p. 211-30. Available from: https://ebookcentral.proquest.com/lib/chalmers/detail.action?docID=1791862.

[79] PubChem [Internet]. Bethesda (MD): National Library of Medicine (US), National Center for Biotechnology Information; 2004-. Sodium Hydroxide. [cited 2023 Mar 3]. Available from: https://pubchem.ncbi.nlm.nih.gov/compound/Sodium-hydroxide.

[80] Wang Y. Cellulose fiber dissolution in sodium hydroxide solution at low temperature: dissolution kinetics and solubility improvement [Dissertation on the Internet]. Georgia: Georgia Institute of Technology; 2008 [cited 2023 Apr 3]. Available from: https://smartech.gatech.edu/bitstream/handle/1853/26632/wang_ying_200812_phd.pdf?sequence=1&isAllowed=y.

[81] PubChem [Internet]. Bethesda (MD): National Library of Medicine (US), National Center for Biotechnology Information; 2004-. Hydrochloric Acid. [cited 2023 Mar 3]. Available from: https://pubchem.ncbi.nlm.nih.gov/compound/313.

[82] PubChem [Internet]. Bethesda (MD): National Library of Medicine (US), National Center for Biotechnology Information; 2004-. Sodium Chloride. [cited 2023 Mar 3]. Available from: https://pubchem.ncbi.nlm.nih.gov/compound/5234.

[83] Wei W, Xu J, Chen W, Mi L, Zhang J. A review of sodium chloride-based electrolytes and materials for electrochemical energy technology. J Mater Chem A [Internet]. 2022 [cited 2023 Mar 16];10(6):2637-71. DOI: 10.1039/D1TA09371A.

[84] PubChem [Internet]. Bethesda (MD): National Library of Medicine (US), National Center for Biotechnology Information; 2004-. Sucrose. [cited 2023 Mar 3]. Available from: https://pubchem.ncbi.nlm.nih.gov/compound/5988.

[85] Procter & Gamble, Sverige AB. Blandning Yes Original. [Internet]; 2023 [cited 2023 Mar 6]. Available from: https://www.tingstad.com/se-en/fixed/productdocument/safetydatasheet/564538.pdf.

[86] PubChem [Internet]. Bethesda (MD): National Library of Medicine (US), National Center for Biotechnology Information; 2004-. GHS Classification. [cited 2023 Mar 6]. Available from: https://pubchem.ncbi.nlm.nih.gov/ghs/.

[87] George FM. pH values of common drinks [Internet]. The International Journal of Dental Clinics; 2021 [cited 2023 May 9]. Available from: https://www.sheltondentistry.com/patient-information/ph-values-common-drinks/.

[88] Facts CS. Sodium Hydroxide [Internet]. US: American Chemistry Council, Inc; 2022 [cited 2023 May 9]. Available from: https://www.chemicalsafetyfacts.org/chemicals/sodium-hydroxide/.

[89] Guneser O, Hosoglu MI, Guneser BA, Yuceer YK. 1 - Engineering of Milk-Based Beverages: Current Status, Developments, and Consumer Trends. In: Grumezescu AM and Holban AM, editors. Milk-Based Beverages [Internet]. Netherlands: Woodhead Publishing; 2019 [cited 2023 May 9]. p. 1-37. DOI: 10.1016/B978-0-12-815504-2.00001-3.

[90] Ica Maxi. Apelsin Vätskeersättning Brustablett 20p ICA Hjärtat [Internet]. Gothenburg: Sweden: Ica Maxi; c 2022 [cited 2023 May 9]. Available from: https://handlaprivatkund.ica.se/stores/1004219/products/Apelsin-V%C3%A4tskeers%C3%A4ttning-Brustablett-20p-ICA-Hj%C3%A4rtat/1505975.

[91] Coca-Cola Sverige . Coca-Cola är världens mest välkända och älskade läskedryck [Internet]. Stockholm: Sweden: Coca-Cola AB; c 2020 [cited 2023 May 9]. Available from: https://www.coca-cola.se/vara-varumarken/coca-cola.

[92] Schindelin J, Arganda-Carreras I, Frise E et al . Fiji: an open-source platform for biological-image analysis. Nat Methods [Internet]. 2012 [cited 2023 May 17];9:676–682. DOI: 10.1038/nmeth.2019.

[93] Bundy WM, Ishley JN. Kaolin in paper filling and coating. Appl Clay Sci [Internet]. 1991;5(5):397-420. DOI: 10.1016/0169-1317(91)90015-2.

[94] Rivera O, Pavez O, Kao JL, Nazer A. Metallurgical characterization of kaolin from Atacama, Chile. REM - International Engineering Journal [Internet]. 2016 [cited 2023 May 3] Oct;69(4):473-8. DOI: ://doi.org/10.1590/0370-44672016690005.

[95] Leroy P, Lassin A, Azaroual M, André L. Predicting the surface tension of aqueous 1:1 electrolyte solutions at high salinity. Geochim Cosmochim Acta [Internet]. 2010 [cited 2023 May 3];74(19):p. 5427-42. DOI: 10.1016/j.gca.2010.06.012.

[96] Liang S, Wu J, Tian H, Zhang L, Xu J. High-Strength Cellulose/Poly(ethylene glycol) Gels. ChemSusChem [Internet]. 2008 [cited 2023 May 10];1(6):558-63. DOI: 10.1002/cssc.200800003.

[97] Lindman B, Medronho B, Alves L, Costa C, Edlund H, Norgren M. The relevance of structural features of cellulose and its interactions to dissolution, regeneration, gelation and plasticization phenomena. Phys Chem Chem Phys [Internet]. 2017 [cited 2023 Mar 4];19(35):23704-18. DOI: 10.1039/C7CP02409F.

[98] Maurer HW. Chapter 18 - Starch in the Paper Industry. In: BeMiller J and Whistler R, editors. Starch (Third Edition) [Internet]. San Diego: USA; Elsevier: Academic Press; 2009 [cited 2023 May 10]. p. 657-713. DOI: 10.1016/B978-0-12-746275-2.00018-5.

[99] Vinnova. Real time 4D X-ray microtomography Imaging and analysis of water transport mechanisms in sustainable paper straws [Internet]. Stockholm: Vinnova; 2021 [cited 2023 May 19]. Available from: https://www.vinnova.se/p/real-time-4d-x-ray-microtomography-imaging-and-analysis-of-water-transport-mechanisms-in-sustainable-paper-straws.

[100] PubChem [Internet]. Bethesda (MD): National Library of Medicine (US), National Center for Biotechnology Information; 2004-. Pure Water Density Standard, UKAS ISO/IEC17025 and ISO Guide 34 certified, density: 0.9982 g/mL at 20 C, density: 0.9970 g/mL at 25 C. [cited 2023 May 9]. Available from: https://pubchem.ncbi.nlm.nih.gov/substance/329798918.

[101] Merck. Polyethylene glycol 3000 [Internet]. Darmstadt: Merck KGaA; c 2023 [cited 2023 May 9]. Available from: https://www.merckmillipore.com/SE/en/product/Polyethylene-glycol-3000,MDA_CHEM-817019?ReferrerURL=https%3A%2F%2Fwww.google.com%2F.

[102] Merck. Polyethylene glycol 35000 [Internet]. Darmstadt: Merck KGaA; c 2023 [cited 2023 May 9]. Available from: https://www.merckmillipore.com/SE/en/product/Polyethylene-glycol-35000,MDA_CHEM-818892?ReferrerURL=https%3A%2F%2Fwww.google.com%2F.

[103] Fisher Scientific. Hydrochloric Acid Solution, Volumetric, 1M HCl (1N), Honeywell™ Fluka™ [Internet]. Pittsburgh: Fisher Scientific; c 2023 [cited 2023 May 9]. Available from: https://www.fishersci.com/shop/products/hydrochloric-acid-solution-volumetric-1m-hcl-1n-honeywell-fluka/60047399.

[104] Fisher Scientific. Sodium Hydroxide, 0.1M, Chemlab™ [Internet]. Pittsburgh: Fisher Scientific; c 2023 [cited 2023 May 9]. Available from: https://www.fishersci.pt/shop/products/sodium-hydroxide-0-1m-3/12536548.

[105] Sigma-Aldrich. Tween®20 SÄKERHETSDATABLAD [Internet]. Pittsburgh: Merck Life Science AB; 2021 [cited 2023 May 9]. Available from: https://www.sigmaaldrich.com/SE/sv/sds/sigma/p2287.

A

Appendix 1

A dilution series with Yes was evaluated. The first concentration evaluated was a 20wt% Yes solution since the behaviour of an extreme was desired. The concentrations was too high for the CLSM method used in this project since the liquid was penetrating throughout the whole cross-section of the paper material faster than the CLSM image capturing rate every 3rd second. Therefore a liquid with a lower concentration, 5wt%, of Yes was evaluated. The same course was identified for this concentration. However, pH and viscosity were measured for these liquids and the results can be seen in Table A.1. Three liquids with even lower concentrations, 0.1wt%, 0.05wt% and 0.01wt% of Yes, were therefore evaluated. At these concentrations, it was possible to capture images close enough to identify the liquid front penetrating through the cross-section of the paper.

Table A.1: *Higher concentrations of Yes that were evaluated in CLSM experiments.*

Liquid	**pH**	**Viscosity** $[10^{-3}\mathbf{Pa \cdot s}]$	**Density** $[\mathbf{g/cm^3}]$
Yes 20wt%	9.13	11.78	1.01
Yes 5wt%	9.13	1.19	1.00

A.1 Density calculations for liquids

The density for the liquids was calculated according to the formula which applies to binary mixtures, presented as Equation (A.1).

$$D = (X_1 \cdot D_1) + (X_2 \cdot D_2) \tag{A.1}$$

, where D is the density of the binary mixture, X_1 and X_2 are the mass fractions of components 1 and 2, and D_1 and D_2 are the density of components 1 and 2. The density of water is 0.997 g/cm^3 at 25°C [100].

The density was calculated in two steps. In the first step, the modifiers were mixed with water in a concentration twice as high as the desired final concentration, as described in Section 3.2.1.4. The densities and parameters for these solutions are presented in Table A.2

Table A.2: *Density calculations made in the first step for the concentrations twice as high as the desired final concentrations.*

Liquid	$\mathbf{X_1}$	$\mathbf{D_1}$ **[c/cm^3]**	$\mathbf{X_2}$	$\mathbf{D_2}$ **[c/cm^3]**	$\mathbf{D_{binaryliquid}}$ **[g/cm^3]**
PEG 3000	0.230	1.21 [101]	0.770	0.997	1.046
PEG 35000	0.231	1.20 [102]	0.769	0.997	1.044
pH 2	0.021	1.10 [103]	0.979	0.997	0.999
pH 9	0.002	0.84 [104]	0.998	0.997	0.997
Tween®20 (>CMC)	0.0003	1.10 [105]	0.9997	0.997	0.997
Tween®20 (<CMC)	0.0001	1.10 [105]	0.9999	0.997	0.997
Yes 20wt%	0.400	1.03 [85]	0.600	0.997	1.011
Yes 5wt%	0.101	1.03 [85]	0.899	0.997	1.001
Yes 0.1wt%	0.002	1.03 [85]	0.998	0.997	0.997
Yes 0.05wt%	0.001	1.03 [85]	0.999	0.997	0.997
Yes 0.01wt%	0.002	1.03 [85]	0.998	0.997	0.997
NaCl	0.007	2.17 [82]	0.993	0.997	1.005
Saccharose	0.197	1.59 [84]	0.803	0.997	1.114

The densities for the base solutions calculated in Table A.2 was used as D_1 in Table A.3, to calculate the final concentrations of the modified liquids, again by using Equation (A.1).

Table A.3: *Density calculations made in the second step for the final concentrations of the modified liquids used in the CLSM experiments.*

Liquid	$\mathbf{X_1}$	$\mathbf{D_1}$ **[c/cm^3]**	$\mathbf{X_2}$	$\mathbf{D_2}$ **[c/cm^3]**	$\mathbf{D_{binaryliquid}}$ **[g/cm^3]**
PEG 3000	0.514	1.046	0.486	0.997	1.022
PEG 35000	0.496	1.044	0.504	0.997	1.020
pH 2	0.498	0.999	0.513	0.997	1.009
pH 9	0.500	0.997	0.500	0.997	0.997
Tween®20 (>CMC)	0.498	0.997	0.502	0.997	0.997
Tween®20 (<CMC)	0.507	0.997	0.493	0.997	0.997
Yes 20wt%	0.505	1.011	0.495	0.997	1.014
Yes 5wt%	0.497	1.001	0.503	0.997	0.999
Yes 0.1wt%	0.492	0.997	0.508	0.997	0.997
Yes 0.05wt%	0.502	0.997	0.498	0.997	0.997
Yes 0.01wt%	0.504	0.997	0.496	0.997	0.997
NaCl	0.504	1.005	0.496	0.997	1.001
Saccharose	0.486	1.114	0.514	0.997	1.054

A.2 Transport mechanism for Yes

A1 and A2 in Figure A.1, show pictures from one CLSM experiment where a 0.1wt% solution of Yes was used and in B1 and B2 a 0.01wt% Yes is used. A1 and B1 show the cross-section of the paper in green and the pore space in black before the liquids were added. A2 and B2 show the cross-section of the paper, in green, when it has been in contact with the liquid for 72s and 141s respectively, shown in orange colour. It can be seen in both cases that the pore space is filled with liquid, which indicates that the liquid is primarily transported through the pores and the mechanism of capillary transport in the pore space occur.

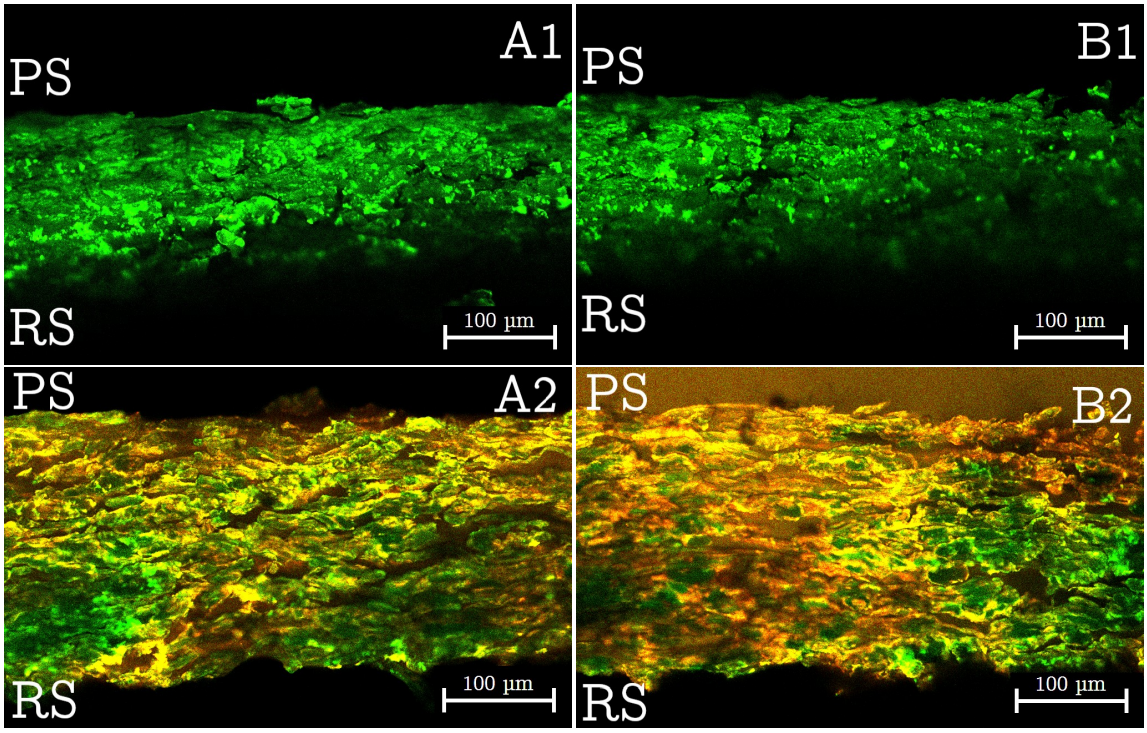

Figure A.1: *Images of mass transport mechanisms for Yes 0.1wt% in A1 and A2, and Yes 0.01wt% in B1 and B2. The time difference between A1 and A2 is 72s and it is 141s between B1 and B2. PS and RS are marked in the images showing the print side and reversed side of the cross-section of the paper.*

DEPARTMENT OF CHEMISTRY AND CHEMICAL ENGINEERING
CHALMERS UNIVERSITY OF TECHNOLOGY
Gothenburg, Sweden 2023
www.chalmers.se

CHALMERS
UNIVERSITY OF TECHNOLOGY